第 54 卷第 1 期
2026 年 1 月

硅 酸 盐 学 报
JOURNAL OF THE CHINESE CERAMIC SOCIETY

Vol. 54，No. 1
January，2026

http://jccsoc.cbpt.cnki.net

DOI：10.14062/j.issn.0454-5648.20250616

综 合 评 述

钙钛矿太阳能电池中钙钛矿薄膜的退火工艺

孟文兵[1]，塔伊尔江• 图尔荪[1]，贺明化[1]，张林睿[2,3]，宁 君[2,3]

(1. 新疆和田学院数理学院，新疆 和田 848000；2. 内蒙古师范大学物理与电子信息学院，呼和浩特 010022；3. 内蒙古自治区应用凝聚态物理重点实验室，呼和浩特 010022)

摘 要：钙钛矿太阳能电池(PSCs)因其卓越的光电性能成为光伏领域的研究热点。钙钛矿薄膜作为器件中的光吸收层，直接影响 PSCs 器件的光伏性能。通常情况下，钙钛矿晶体的生长条件是决定钙钛矿薄膜质量的主要因素之一。在高质量钙钛矿晶体的形成过程中，退火的作用主要是去除钙钛矿湿膜中的溶剂并促使薄膜结晶。不同退火方法及工艺对薄膜生长的促进作用也不尽相同。因此，本文综述了总结已报道的钙钛矿晶体生长的主要退火方法，讨论了不同退火工艺下钙钛矿薄膜的结晶质量，并系统地总结了影响退火效果的主要工艺因素。最后，预测了退火工艺在未来钙钛矿太阳能电池商业化发展中的前景。

关键词：钙钛矿太阳能电池；钙钛矿薄膜；退火；结晶质量
中图分类号：O69.5　　**文献标志码**：A　　**文章编号**：0454–5648(2026)03–0328–22
网络出版时间：2025–11–17

钙钛矿材料因其优异的光物理特性在光伏领域备受瞩目，因此有机–无机杂化金属卤化物钙钛矿太阳能电池(PSCs)应运而生。PSCs 从 2009 年发展至今，由最初 3.8%的光电转换效率[1]上升到最近的认证效率 27%[2]，短短十余年间便成为光伏领域的研究热点。

PSCs 的光伏性能受到钙钛矿薄膜质量的直接影响，而退火工艺则是高质量钙钛矿薄膜制备过程的关键环节。热退火工艺被广泛应用到各类太阳能电池的薄膜制备中，已被充分证明是消除残余应力、内部缺陷和调整材料内部微观组织的有效手段[3–4]。例如，硅基太阳能电池中的烧结工艺，即在一定温度下完成退火过程，促成金属/半导体之间的欧姆接触[5]。在砷化镓、铜铟镓硒等太阳能电池中亦有相似的工艺。同样地，在钙钛矿太阳能电池中，退火工艺用于钙钛矿薄膜的相转变和结晶，以提高钙钛矿薄膜质量。然而，通用的热退火工艺造成薄膜针孔、晶粒尺寸不均匀等问题，从而降低了器件的光伏性能。因此，研究人员开发了一些新型退火技术，如溶剂退火[6]、环境空气退火[7]、微波退火[8]、红外退火[9–11]、快速退火[12–13]、湿度环境辅助退火[14]等。此类退火技术集中体现在提升钙钛矿薄膜质量和降低工艺成本上，在低温、短时间内完成钙钛矿薄膜的高质量结晶，从而改善薄膜的形貌和光电性能。

基于此，综述了近年来 PSCs 中钙钛矿薄膜退火工艺的研究进展，重点介绍了钙钛矿薄膜常见的退火方法及影响退火效果的工艺因素。首先，介绍退火工艺及其促进钙钛矿薄膜结晶的机制。其次，讨论了目前已报道的钙钛矿晶体生长的主要退火方法，系统总结了影响退火效果的主要工艺因素，接着讨论了钙钛矿薄膜的无退火技术的发展状况。最后，对钙钛矿薄膜退火工艺未来研究的发展进行展望，希望为钙钛矿太阳能电池的商业化发展提供支持。

1 退火及其对钙钛矿薄膜结晶的影响

1.1 退火与钙钛矿薄膜结晶

在太阳能电池的半导体薄膜的制备过程中，退火通常指的是将半导体薄膜加热到一定温度后，持

收稿日期：2025–07–12。　修订日期：2025–08–19。
基金项目：新疆和田学院 2025 年校级科研培育项目重点项目(2025ZR012)；内蒙古自治区自然科学基金(2023LHMS06015)；内蒙古自治区高等学校科学研究项目(NJZY21568)。
第一作者：孟文兵(1992—)，男，硕士，讲师。
通信作者：宁 君(1983—)，男，博士，副教授。

Received date: 2025–07–12.　**Revised date:** 2025–08–19.
First author: MENG Wenbing (1992–), male, Master, Lecturer.
E-mail: 1151076702@qq.com
Correspondent author: NING Jun (1983–), male, Ph.D., Associate Professor.
E-mail: ningjun@imnu.edu.cn

续一段时间，最后再进行缓慢冷却的工艺，对于改善薄膜材料光学与电学性能具有重要的意义。

在钙钛矿薄膜的制备过程中，退火工艺是必不可少的工艺环节。其主要作用体现在 4 个方面：首先，退火使得钙钛矿薄膜材料发生相变，如溶液旋涂法制备的钙钛矿湿膜经退火后，由原来湿膜中的 δ 相转变为退火后的 α 相，薄膜的光电性能得以大幅提升。其次，在退火过程中，外部能量的输入驱动钙钛矿薄膜内非晶态区域的原子重新排列，从而使晶格呈现出有序性，薄膜中材料由非晶态向晶态转变，增大晶粒尺寸，使晶界更加清晰。再次，退火过程可以帮助去除钙钛矿湿膜中残留的溶剂，同时消除钙钛矿薄膜中的缺陷，减少载流子的非辐射复合，进而增强薄膜的电学性能。最后，经过退火后，钙钛矿薄膜表面形貌得以改善，表面粗糙度降低，薄膜的光学性能增强，同时也有利于太阳能电池器件的后续工艺制备。

1.2　钙钛矿薄膜退火工艺的机理

钙钛矿薄膜的形成过程中，退火工艺主要影响薄膜的晶核生成(成核)和晶粒生长 2 个阶段，这 2 个阶段直接影响着钙钛矿薄膜的均匀性和覆盖率。通常情况下，退火前的钙钛矿薄膜是湿膜，根据文献[15–18]报道，美国化学家 Victor K. LaMer 提出了一种经典的成核与生长模型，称为 LaMer 模型。该理论用于解释单分散纳米颗粒的形成过程，主要分为前驱体积累阶段、爆发式成核阶段和扩散控制生长阶段 3 个阶段。以下结合图 1[18]揭示钙钛矿的成核过程的 3 个阶段：区域 I (成核前)、区域 II (成核)和区域III (生长)。在阶段 I，退火使得溶剂蒸发，导致前驱体浓度随时间增加，尚未达到成核临界饱和浓度；阶段 II 为过饱和阶段，此时浓度达到并超过临界成核浓度，晶核生成。晶核的生成会消耗溶质，湿膜中前驱体溶液浓度会降至低于过饱和极限，成核停止。该阶段成核时间与成核密度密切相关。当成核时间增大时，晶核生成速率降低，导致成核密度较低。当成核时间较短时，可迅速生成大量晶核。在成核阶段获得高密度的均匀晶核有利于晶体的生长质量。因此，在阶段 II 的时间间隔应缩短，以确保晶体核数量的激增；在阶段III，前驱体浓度已降至成核临界浓度以下，前驱体无法产生新的晶核，但剩余的前驱体通过扩散吸附到已有的晶核表面，驱动晶核缓慢生长。

根据以上分析及文献[19]报道，快速成核与缓慢结晶是改善钙钛矿的生长的两条途径。快速成核能保证薄膜的高覆盖率，而缓慢结晶则优化粗糙度和晶粒尺寸。文献中报道的改善钙钛矿薄膜质量的各类退火工艺均与这两条途径直接相关。

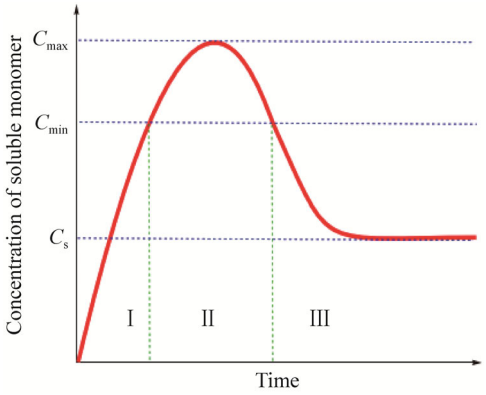


图 1　钙钛矿成核和晶体生长的 LaMer 模型图[18]

Fig. 1　Diagram of the LaMer model for perovskite nucleation and crystal growth[18]

2　钙钛矿薄膜的退火方法

为了系统地总结和分析各种退火方法，将钙钛矿薄膜的退火方法大致分为传统热退火方法和新型退火技术 2 大类。传统热退火方法，即利用加热台对衬底进行加热退火，是目前应用最广泛且方便简单的钙钛矿结晶方法。Qin 等[20]通过原位掠入射广角 X 射线散射测量，揭示了混合钙钛矿 $FA_{0.83}MA_{0.17}Pb(I_{0.83}Br_{0.17})_3$ 的详细结晶过程，确定 3 个相形成阶段：前驱体溶液阶段、六方 δ 相(2H)阶段和包括六方多型(4H、6H)、MAI-PbI_2-DMSO 中间相和钙钛矿 α 相的复合相阶段。研究表明，存在覆盖六方 δ 相(2H)阶段持续时间的“退火窗口”。钙钛矿膜应在“退火窗口”内退火，避免钙钛矿结晶过程中形成六方多型，从而获得良好的器件性能。同时，笔者通过在混合钙钛矿中加入 Cs^+可以控制结晶。密度泛函理论计算表明，充分 Cs^+的钙钛矿体系会在动力学和热力学上促进 α 相的形成，从而绕过第 3 阶段二次相的形成，从而显著延长退火窗口。该研究为操纵钙钛矿结晶途径以获得更高性能提供了有洞察力的指导。为了得到更高质量的钙钛矿薄膜，在热退火处理的基础上进行工艺改进，取得了良好的效果，如梯度热退火、高温快速退火等，如表 1 所示。

传统热退火方式促进了钙钛矿薄膜的相转变和结晶，一定程度上提升钙钛矿薄膜质量，进而提升 PSCs 器件的光伏性能。然而，这种退火方式不可避

免地造成薄膜针孔以及晶粒尺寸不均匀等问题，一定程度上限制了 PSCs 性能的进一步提升。因此，研究者们不断寻找能够完成钙钛矿薄膜退火过程的其他可能，并由此开发出了一系列新型退火技术，如电磁波(红外光、紫外光、激光和微波)退火、超声退火、溶剂退火等退火方式，如表 2 所示。

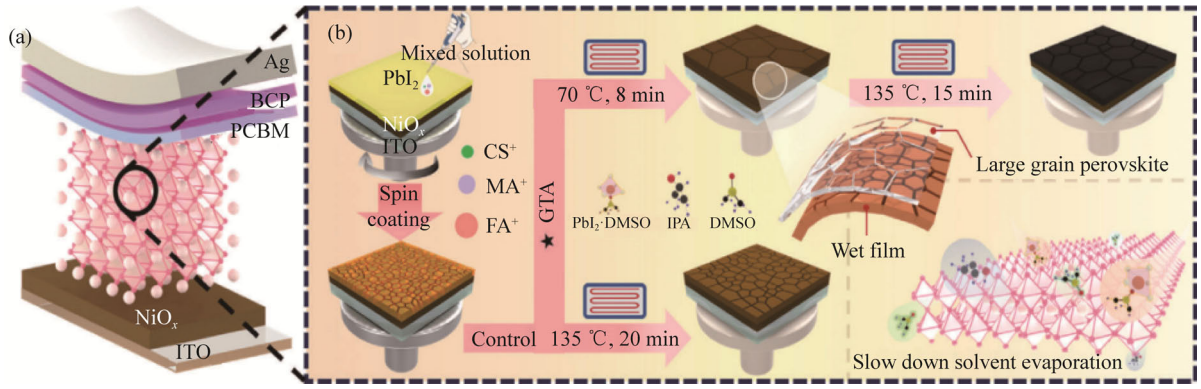


图 2 钙钛矿薄膜的制备工艺和形貌。(a) PSC 结构示意图和(b)一步退火(对照)和梯度热退火方法的实验步骤示意图[21]

Fig. 2 Preparation process and morphology of perovskite thin films. (a) Schematic diagram of PSC structure and (b) experimental steps schematic for one-step annealing (control) and gradient thermal annealing method[21]

表 1 改进后的热退火工艺在钙钛矿薄膜制备中的应用

Table 1 Application of the improved thermal annealing process in the preparation of perovskite thin films

Annealing method	Characteristics
Gradient thermal annealing [21–24]	As depicted in Fig. 2[21], the gradient annealing process reduces the evaporation rate of organic solvents in the wet perovskite film, thereby prolonging the crystallization. Compared to direct annealing, the slower color transition from yellow to black under gradient annealing indicates a reduced crystallization rate. During $MAPbI_3$ annealing[21], the first 5 min of preheating at 60 ℃ see a slow transition of the MAI-PbI_2-DMSO intermediate phase to $MAPbI_3$, accompanied by a gradual dissociation of DMSO which allows for hydrogen bond formation with PbI_2. In contrast, direct thermal annealing completes 90% of both DMSO release and hydrogen bond formation within just 15 s.
Rapid thermal annealing[13,25–26]	While prolonged thermal annealing can induce film decomposition, high-temperature rapid annealing has emerged as a promising alternative. This technique rapidly removes solvent to establish a supersaturated state, thereby promoting perovskite nucleation and increasing crystal nucleus density. It is also cost-effective, environmentally friendly, and highly suitable for large-area perovskite film fabrication. For instance, a 4 s anneal at 400 ℃ can yield grain sizes up to 1 μm[13]. However, the excessively rapid solvent evaporation in this process often causes severe grain contraction, leading to rough surfaces and grain boundary cracks, which ultimately compromise crystal quality.
Synergistic effect of gradient thermal annealing (GTA) and anti-solvent (ATS) [22]	The DMSO was extracted using an anti-solvent to disperse the crystal nuclei, followed by gradient annealing to crystallize the film. This method produced a film with an exceptionally smooth surface, significantly reduced grain boundaries, and grain sizes exceeding 1 μm (Fig. 3[22]). Consequently, both the film quality and device performance were substantially enhanced.
Vacuum-assisted thermal annealing [27]	Compared with the traditional thermal annealing process, vacuum-assisted thermal annealing can accelerate the crystallization of perovskite, resulting in a calcium titanate film without pores, with fewer defect states and high crystallinity, as shown in Fig. 4[27].
Ambient air annealing [7]	As demonstrated in Fig. 5a–Fig. 5d[7], this method is commonly utilized in the annealing process of $CsPbI_3$ films. Remarkably, annealing in ambient air does not degrade the photoelectric properties but instead improves carrier extraction efficiency and suppresses non-radiative interface defects. This work provides a new concept for the annealing of inorganic perovskite films, paving the way for their ambient fabrication.
Hot casting [28–29]	The hot-casting procedure is depicted in Fig. 5(e)[28]. Typically, a preheated (70–100 ℃) perovskite precursor solution is deposited onto a substrate maintained at a higher temperature (100–180 ℃). A substrate temperature above the perovskite crystallization point enables rapid solidification, while the remaining solvent facilitates grain growth. This combination results in a uniform, fully-covered film with large grains. Crucially, the process eliminates the need for a separate post-annealing step, thereby streamlining the fabrication process and ultimately lowering both the cost and production time.

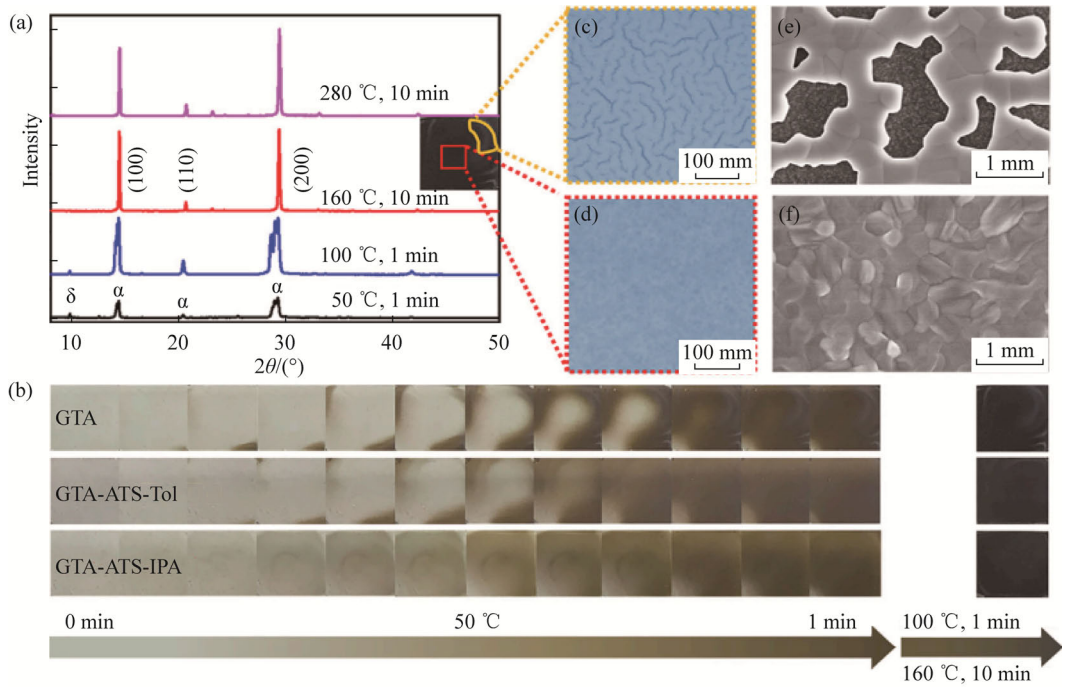


图 3　$CsPbI_2Br$ 晶体生长的反溶剂辅助梯度热退火(GTA)方法[22]。(a)不同梯度温度退火的 $CsPbI_2Br$ 薄膜的 X 射线衍射(XRD)谱；(b) GTA、GTA-ATS-Tol 和 GTA-ATS-IPA 薄膜在 50 ℃下 0～1 min 的颜色演变照片，以及经过 50、100 ℃和 160 ℃ GTA 处理后的照片；(c) GTA 薄膜条纹区域的光学显微镜照片(比例尺，100 mm)；(d) GTA 薄膜中心区域的光学显微镜照片(比例尺，100 mm)；(e) GTA 薄膜条纹区域的 SEM 照片(比例尺，1 mm)；(f) GTA 薄膜中心区域的 SEM 照片(比例尺，1 mm)

Fig. 3　GTA method for $CsPbI_2Br$ crystal growth[22]. (a) X-ray diffraction (XRD) patterns of $CsPbI_2Br$ films annealed at different gradient temperatures. Inset: photograph of GTA film after the gradient 50, 100 and 160 ℃ treatments; (b) Photographs of color evolution of GTA, GTA-ATS-Tol, and GTA-ATS-IPA films treated at 50 ℃ from 0 to 1 min and after the GTA treatment at 50, 100 and 160 ℃; (c) Optical microscope image of the GTA film at local region for stripes (Scale bar, 100 mm); (d) Optical microscope image of the GTA film at local region for center (Scale bar, 100 mm); (e) SEM image of the GTA film at local region for stripes (Scale bar, 1 mm); (f) SEM image of the GTA film at local region for center (Scale bar, 1 mm)

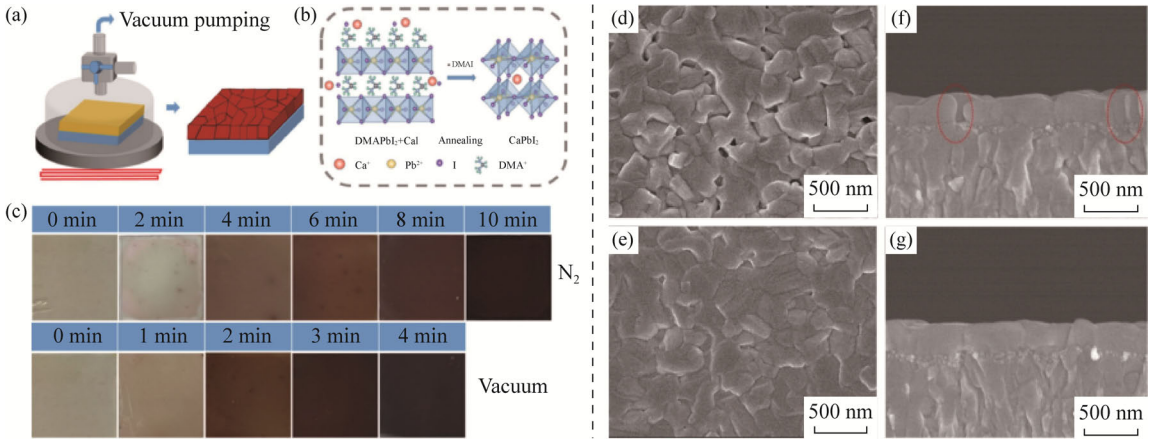


图 4　(a) $CsPbI_3$ 钙钛矿薄膜的真空辅助热退火(VATA)示意图。(b)一维 $DMAPbI_3$ 薄膜通过 Cs^+和 DMA^+之间的阳离子交换转化为三维 $CsPbI_3$ 的机理图。(c)在 N_2 或真空中不同时间退火的 $CsPbI_3$ 薄膜的照片。(d)在氮气中退火的 $CsPbI_3$ 薄膜表面 SEM 照片和(e)真空退火的 $CsPbI_3$ 薄膜表面 SEM 照片；(f)在氮气中退火的 $CsPbI_3$ 薄膜的截面 SEM 照片和(g)真空退火的 $CsPbI_3$ 薄膜的截面 SEM 照片[27]

Fig. 4　(a) Schematic illustration of vacuum-assisted thermal annealing (VATA) for $CsPbI_3$ perovskite film. (b) Mechanism diagram for the conversion of one-dimensional $DMAPbI_3$ film to three-dimensional $CsPbI_3$ through cations exchange between Cs^+ and DMA^+. (c) Photoographs of the $CsPbI_3$ films annealed in the N_2 or vacuum at different times. Top-surface SEM images of the $CsPbI_3$ films annealed in (d) N_2 and (e) vacuum. Cross-sectional SEM images of the $CsPbI_3$ films annealed in (f) N_2 and (g) vacuum[27]

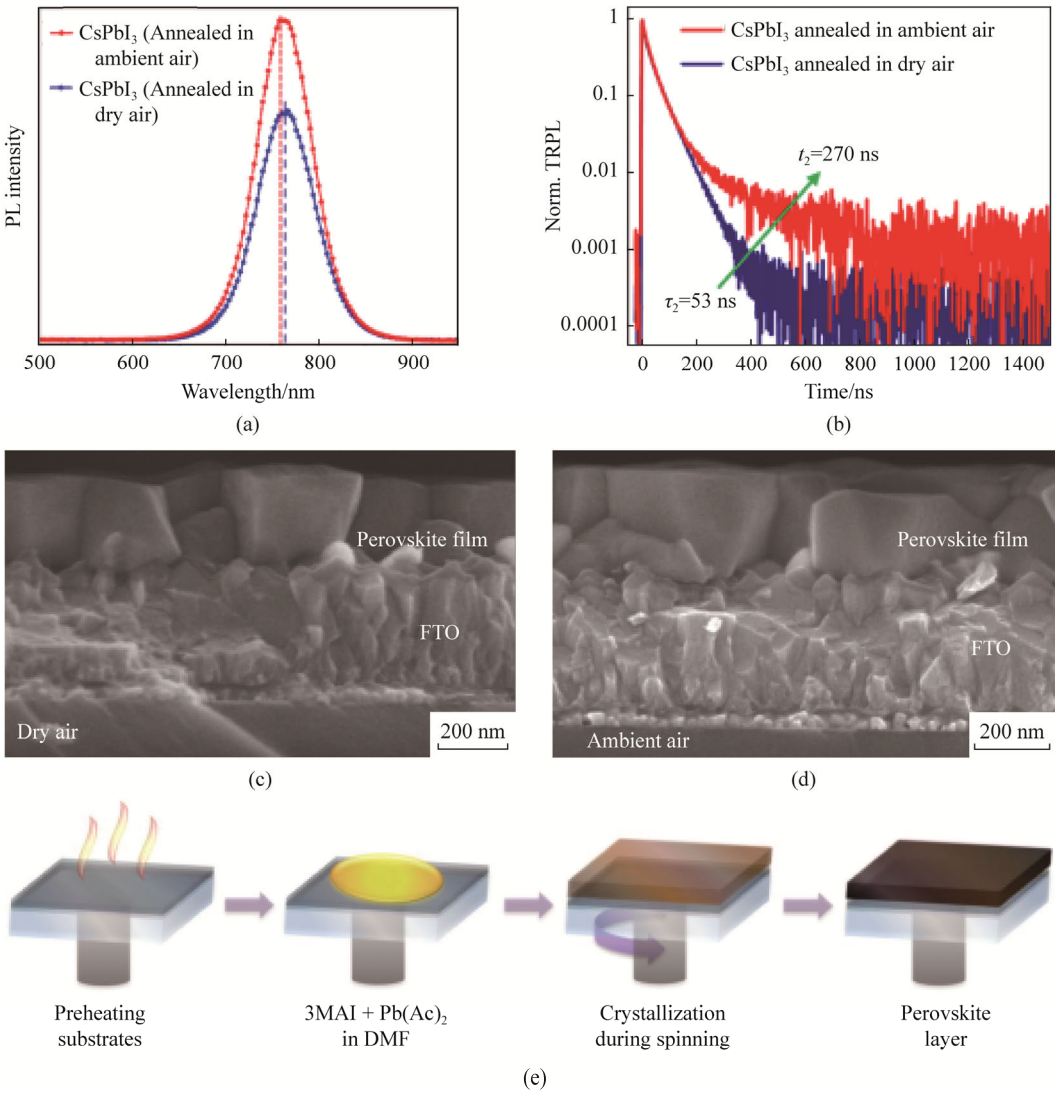


图 5 (a)干燥空气和环境空气退火 $CsPbI_3$ 吸收剂的稳态光致发光发射光谱；(b)干燥空气和环境空气退火 $CsPbI_3$ 薄膜的时间分辨光致发光(TRPL)衰减；在 FTO/TiO_2-C 基底上沉积了干燥空气(c)和环境空气(d)退火 $CsPbI_3$ 吸收膜的横截面 SEM 照片[7]；(e)环境气氛下的热铸法制备钙钛矿结晶层的工艺流程[28]

Fig. 5 (a) Steady-state photoluminescence emission spectra of dry air and ambient air annealed $CsPbI_3$ absorbers; (b) Time-resolved photoluminescence (TRPL) decay of dry air and ambient air annealed $CsPbI_3$ films; Cross-sectional SEM images of dry air (c) and ambient air, (d) annealed $CsPbI_3$ absorber films were deposited on FTO/TiO_2−C substrates[7]; (e) Processing scheme for crystalline perovskite layers, through hot casting under ambient atmosphere[28]

3 退火工艺参数对钙钛矿薄膜的影响

3.1 退火温度

退火使得钙钛矿薄膜内部离子重新排列，其中，铅离子对退火时间和温度有明显影响[55]。在钙钛矿形成过程中，不同铅卤化物与卤化物阳离子自由解离和结合所需能量不同。因此，不同阳离子和卤素组成的钙钛矿材料的退火温度大不相同。有机阳离子的存在导致多数有机无机杂化钙钛矿退火温度低于 150 ℃[56–60]。如 $MAPbI_3$ 的退火温度通常为 150 ℃[57–58]，$FAPbI_3$ 的退火温度也不超过 150 ℃[59]，$Cs_{0.15}FA_{0.85}PbI_3$ 的最佳退火温度也为 150 ℃[60]。对于无机钙钛矿薄膜，退火处理温度远高于 150 ℃。如 $CsPbI_3$ 的退火温度范围为 300～370 ℃[61]，与其他钙钛矿相比，$CsPbI_3$ 具有更好的热稳定性[62–63]。

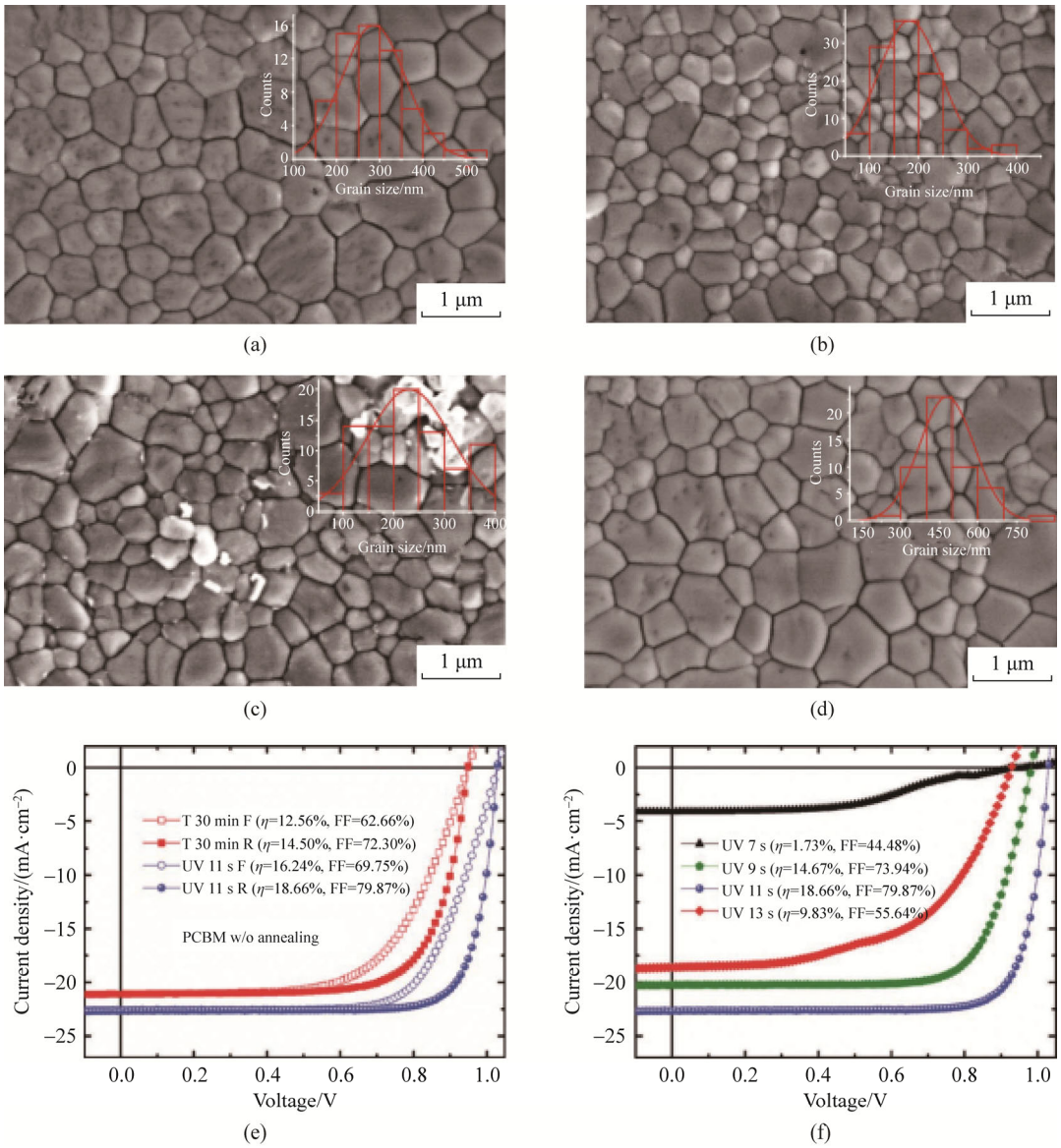
Taguchi 等[64]通过控制钙钛矿 $MAPbI_3$ 层的退火温度，发现对于在约 200 ℃高温退火的钙钛矿层，钙钛矿晶体密集形成，钙钛矿层的表面覆盖率得到提高。Chang 等[65]分别在 80、100、120 ℃和 140 ℃的退火温度下制备了 $MAPbI_3$ 薄膜，并制备了结构为 Ag/spiro-OMeTAD/$CH_3NH_3PbI_3$($MAPbI_3$)/PCBM/

介孔 TiO_2/TiO_2/FTO 的 PSCs 器件，如图 9a～图 9h 所示，钙钛矿的形态和尺寸明显取决于退火温度。高温形成具有随机取向的大钙钛矿晶粒，表面膜稀疏不均匀地形成方形晶体。随着温度的变化，可以看出在接近 100 ℃时制备的钙钛矿薄膜致密平坦。符祥等[66]通过调控 $CsPbI_2Br$ 薄膜的退火温度，制备了碳基全无机钙钛矿太阳能电池器件。研究发现升高退火温度可有效改善 $CsPbI_2Br$ 薄膜的结晶质量，并减少了表面的孔洞，如图 9i 和图 9j 所示，同时器件的光伏性能有显著提高。

表 2　新型退火技术在钙钛矿薄膜制备中的应用

Table 2　Application of new annealing techniques in the preparation of perovskite thin films

Annealing method		Characteristics
Electromagnetic wave annealing	Infrared annealing [9–10, 30–33]	Infrared annealing utilizes its capability to deliver intense energy rapidly, effectively promoting precursor reactions and driving grain growth. As shown in Fig. 6a–Fig. 6d[10], film growth rate and quality are strongly dependent on the infrared photon flux. After 5 min annealing at 940 nm under different light intensities, the resulting surface morphologies were characterized. The results indicate that under identical wavelength and duration, the film processed under 15.80 suns exhibits smoother, more uniform grains with sizes of approximately 450 nm, and a more complete reaction between MAI and PbI_2.
	Ultraviolet (UV) light-annealing[34]	It is generally believed that the high energy of ultraviolet light can decompose perovskite, so the use of ultraviolet light for annealing perovskite films is very rare. As shown in Fig. 6e–Fig. 6f [34], by controlling the amount of UV light exposure, and appropriately utilizing the high absorption of perovskite in the ultraviolet band, crystallization can also be promoted.
	Lasers annealing [35–38]	Studies have shown that lasers can generate temperatures exceeding 100 ℃ within the film. After laser annealing, the film exhibits excellent crystallinity and orientation. Moreover, different wavelengths of lasers have different effects on the growth of the film. The grains have a better grain size at 450 nm, which may be due to the high absorption of calcium titanate at non-UV short wavelengths [37]. The local temperature gradient generated by the laser at the calcium titanate grain boundaries will cause larger grains to absorb more energy, while smaller grains have a higher temperature, thereby inducing the selective growth of larger grains.
	Microwaves annealing [8, 39–41]	The wavelength range of microwaves is from 1 mm to 1 m. Studies have shown that microwaves can effectively control the crystallization of perovskite. By replacing the traditional thermal annealing process (HAP) with the rapid microwave annealing process (MAP), the processing time of perovskite is reduced to less than 1 min. The microwave radiation method can effectively eliminate impurities, thereby achieving large grains of >1 μm in perovskite films, as shown in Fig. 7a–Fig. 7f [41]. This enables the photoelectric conversion efficiency of inverted planar PSC to increase from 18.33% (HAP) to 21.59% (MAP), and it achieves good stability of >1000 h under environmental conditions without the need for encapsulation[41].
Ultrasonic annealing [42–43]		Ultrasound-induced crystallization is also a new type of annealing method. Usually, after preparing the calcium phosphate wet film, ultrasound-induced crystallization is carried out for a period of time. As shown in Fig. 7g–Fig. 7h [43], the calcium phosphate film subjected to ultrasound annealing (15 W-3 min) has a relatively dense grain structure with larger grain sizes (average: 670 nm); while the calcium phosphate film subjected to thermal annealing contains a large number of smaller grains, with occasional larger grains (average 315 nm). These small grains cause vacancies at the grain boundaries, making the calcium phosphate layer susceptible to overheating oxygen and humidity. The smaller particles with a bright sheet-like appearance may represent regions rich in PbI_2. This method can be used for processing the crystallization of calcium phosphate films for flexible devices, as well as for the fabrication process of large-area devices.
Solvent-bath annealing [6, 44]		By utilizing the principle of mutual solubility of organic solvents, specific organic reagents were selected to extract the polar solvents within the perovskite films to facilitate crystallization. In 2025, Wang *et al*.[6] applied fluorocarbon-based solvents for a new type of solvent bath annealing. By comparing two fluorocarbon solvents, perfluoronaphthalene (PFD) and perfluorotoluene (PFT), they investigated the previously overlooked solvent-to-solvent interactions between fluorocarbon compounds and the precursor solvents of perovskite. By increasing the solvent-solvent interactions, high-quality perovskite films with higher crystallinity and fewer film defects were obtained, as shown in Fig. 8[6]. The solar cells annealed with PFT exhibited a high photoelectric conversion efficiency of 24.26%, and the device stability was significantly improved. At a humidity level of 40%–45%, without encapsulation, it maintained 80% of its initial efficiency after 70 d.
Solvent-vapor assisted annealing [45–54]		By adding polar solvent vapor during the annealing process, the solvent vapor is allowed to condense on the surface and grain boundaries of the perovskite film. The condensed solvent dissolves the perovskite on the surface and grain boundaries, providing a liquid medium for the diffusion of the constituent ions, resulting in the fusion of grains, the formation of larger grains and the reduction of grain boundaries[48–49], such as methylamine[50–51], as well as alcohols like ethanol[52], n-butanol[53] and benzoic alcohol[54].



η is photoelectric conversion efficiency; FF is fill factor.

图 6 钙钛矿薄膜在相同温度下在 2 个波长(a) 940 nm 和(b) 850 nm 下以及在相同波长(c) 940 nm-12.60 suns-5 min 和(d) 940 nm-15.80 suns-5 min 下的 SEM 照片[10]；(e) 热退火和紫外退火 PSCs 的性能比较；(f) 仅对 PVSK 层以 7～13 s 的不同 UV 退火时间 PSCs 的电流密度–电压(*J*–*V*)特性[34]

Fig. 6 SEM images of the perovskite film at the same temperature in two wavelengths (a) 940 nm and (b) 850 nm, and at the same wavelengths (c) 940 nm-12.60 suns-5 min and (d) 940 nm-15.80 suns-5 min[10]. (e) Performance comparison between thermal-annealed and ultraviolet (UV)-annealed PSCs; (f) the current density–voltage (*J*–*V*) characteristics of PVSCs in reverse scan with different UV annealing time from 7 s to 13 s on the perovskite solar cells (PSCs) active layer only [34]

Cao 等[25]研究了退火温度对 $CH_3NH_3PbI_3$ 钙钛矿薄膜的影响。钙钛矿薄膜的扫描电子显微镜(SEM)照片(见图 10a～图 10f)清楚地表明，晶粒尺寸强烈依赖退火温度。当退火温度从 100 ℃升高到 250 ℃时，平均晶粒尺寸从 217.6 nm 增加到 431.9 nm (见图 10a 和图 10e)。250 ℃时退火时间优化为 10 s，以避免钙钛矿薄膜发生显著分解。随着退火温度的升高，晶粒微观结构从小晶粒演变为柱状晶粒(见图 10b、图 10d、图 10f)。

合适的退火温度能够促进钙钛矿结晶，进而提升器件性能。然而，过高的退火温度容易造成钙钛矿分解，导致器件性能恶化。Wargulski 等[67]在研究 $(Cs_{0.22}FA_{0.78})Pb(I_{0.85}Br_{0.15})_3$ 中添加了 5% (摩尔分数)的 $MAPbCl_3$ 的三卤化物钙钛矿薄膜的退火工艺时，发现器件的光电转换效率(PCE)对退火温度有很强的相关性。当退火温度从 125 ℃升到 170 ℃时，器件性能恶化，原因是开路电压(V_{oc})和填充因子(FF)明显下降。研究发现钙钛矿薄膜表面存在 PbI_2 片晶，

从图 10g 可以看出，薄膜表面 PbI_2 片晶的分布面积随着退火温度的升高而增加。当退火温度从 125 ℃升高到 170 ℃时，器件性能恶化的原因是 PbI_2 片晶引起的串联电阻增加和界面复合增加，导致太阳能电池器件的 V_{oc} 和 FF 降低。该项研究的相关分析为解决钙钛矿太阳能电池的热稳定性问题提供了新的支持。

3.2　退火时间

钙钛矿薄膜的持续退火时间对薄膜的性能有显著的影响。当退火短暂(＜10 min)时，钙钛矿薄膜往往结晶不充分，有大量非晶区域残留，导致薄膜的光学和电学性能均较差，且缺陷较多，由此制得的 PSCs 器件性能较差。退火时间适当(10～30 min)时，薄膜中晶粒均匀生长，非晶区域极少，且缺陷在退火过程中得到修复；薄膜光滑平整，其光学和电学性能优异，导致 PSCs 器件光伏性能比较突出。然而长时间(＞30 min)退火往往造成薄膜中钙钛矿分解产生 PbI_2，如图 11a 和图 11b 所示[68]，导致光电性能变差；由图 11c 和图 11f 可知，随着退火时间延长，薄膜由光滑平整逐渐变得粗糙，导致器件性能逐步下降[68]。

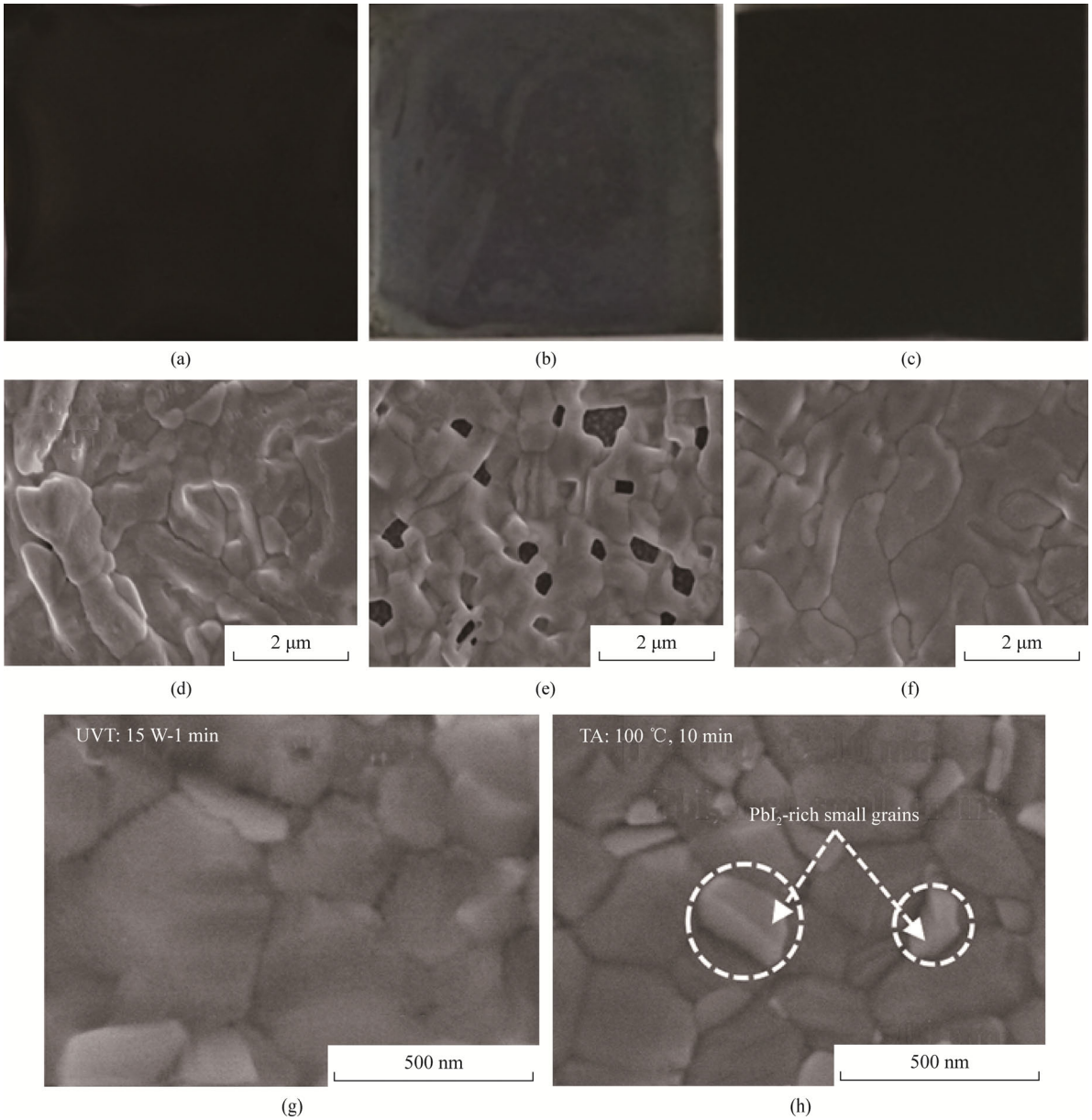


图 7　(a，d)空气条件下微波辐射，(b，e)空气条件下加热退火和(c，f)惰性气氛下加热退火的钙钛矿薄膜的照片和俯视 SEM 照片[41]；分别通过(g)超声退火(15 W-1 min)和(h)热退火(100 ℃，10 min)制备的钙钛矿薄膜的 SEM 照片[44]

Fig. 7　Photographs and top view SEM images of perovskite films fabricated by microwave radiation in (a, d) air condition (MRAC), (b, e) heating-annealing in air condition (HAAC) and (c, f) heating-annealing in inert atmosphere (HAIA)[41]. SEM images of perovskite films made by (g) UVT (15 W-1 min) and (h) TA (100 ℃, 10 min), respectively[44]

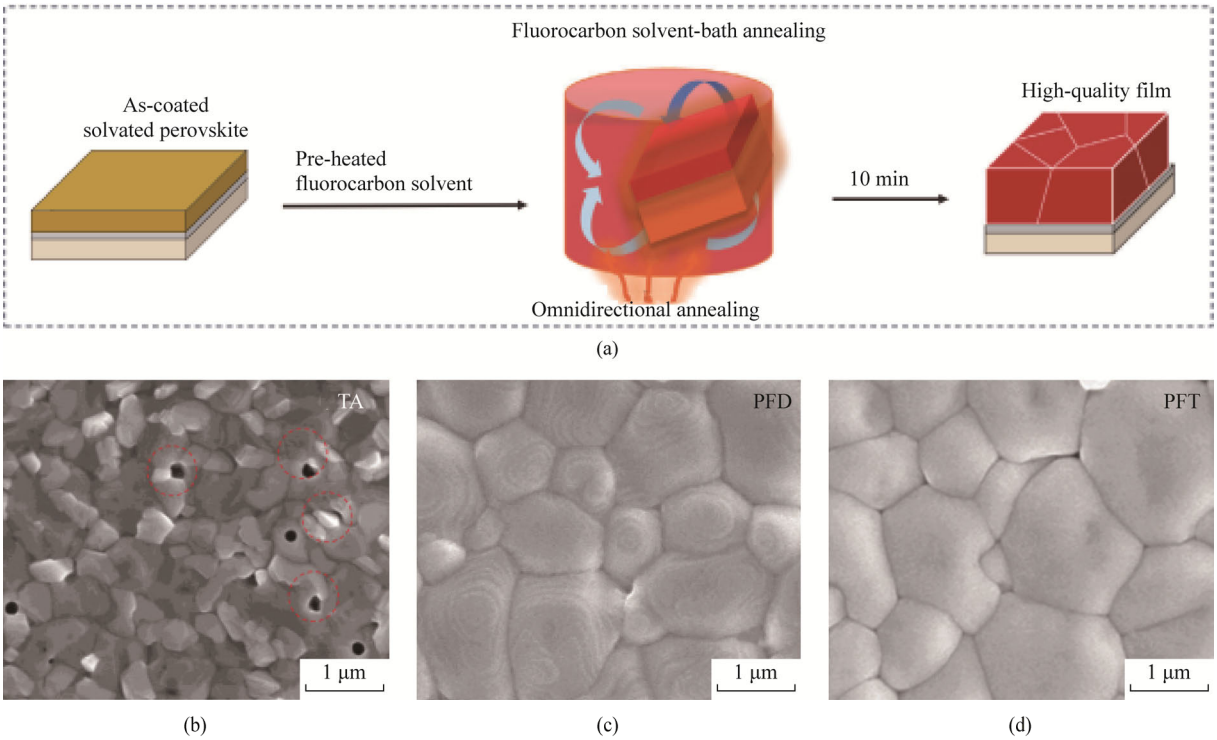


图 8 (a)钙钛矿薄膜溶剂浴退火工艺的图示，(b)热退火(TA)、(c)全氟萘烷(PFD)和(d)全氟甲苯(PFT)溶剂浴退火钙钛矿薄膜的俯视 SEM 照片[6]

Fig. 8 (a) Illustration of solvent-bath annealing process for perovskite films. Top-view SEM images of (b) Thermally annealed (TA), (c) Perfluorodecalin (PFD), and (d) Perfluorotoluene (PFT)-annealed perovskite films [6]

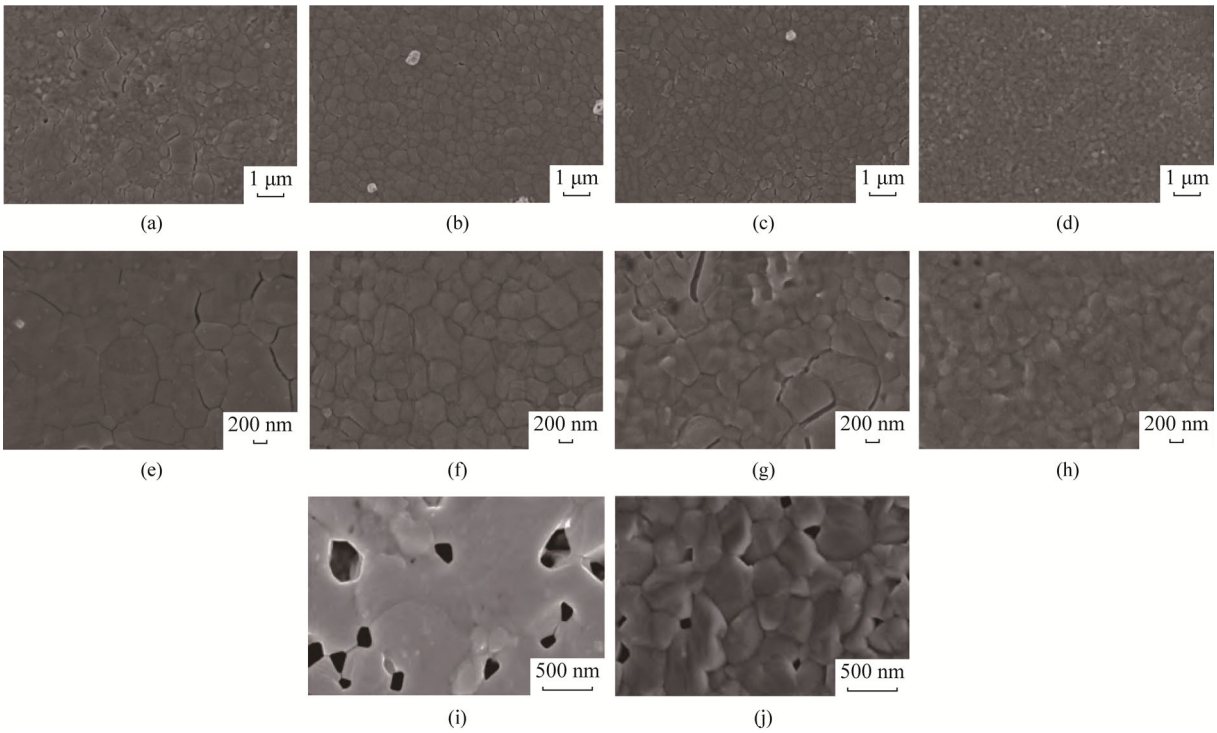


图 9 不同退火温度下 $MAPbI_3/TiO_2$/FTO 结构的 FE-SEM 照片，(a，e)，(b，f)，(c，g)，(d，h)，分别为 80、100、120 和 140 ℃退火的低倍和高倍照片[65]；(i，j)分别为 260、280 ℃退火温度处理的 $CsPbI_2Br$ 钙钛矿薄膜 SEM 照片[66]

Fig. 9 FE-SEM images of the top view of the $MAPbI_3/TiO_2$/FTO structure at different annealing temperatures, (a,e), (b,f), (c,g), (d,h), low and high magnifications annealed at 80, 100, 120 ℃, and 140 ℃[65]; (i, j) SEM images of $CsPbI_2Br$ perovskite film annealed at 260 and 280 ℃, respectively[66]

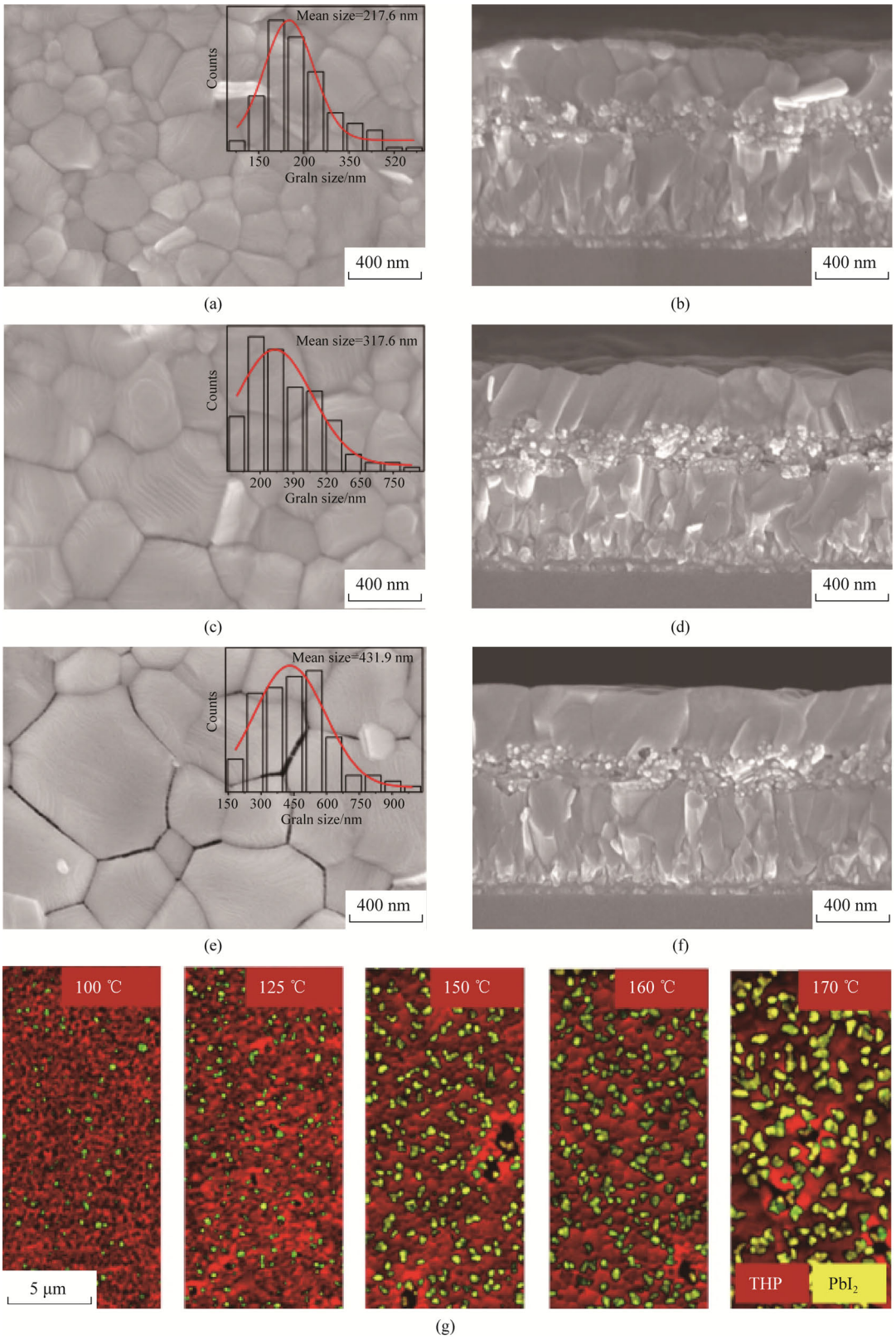


图 10　不同温度退火处理后的钙钛矿薄膜的表面(左)和截面(右) SEM 照片[25]。(a)和(b) 100 ℃退火 20 min，(c)和(d) 175 ℃退火 60 s，(e)和(f) 250 ℃退火 10 s (插图是相应钙钛矿薄膜的晶粒分布)；(g)钙钛矿薄膜的阴极发光(CL)图[67]，对应钙钛矿(红色)和 PbI_2 (黄色)组成

Fig. 10　Surface (left) and cross-sectional (right) SEM images of the perovskite films annealed at different temperature[25]. (a) and (b) 100 ℃ for 20 min, (c) and (d) 175 ℃ for 60 s, (e) and (f) 250 ℃ for 10 s. Insets are grain distribution of the corresponding perovskite films. (g) Cathodoluminescence (CL) diagram of perovskite film [67], corresponding to perovskite (red) and PbI_2 (yellow) composition

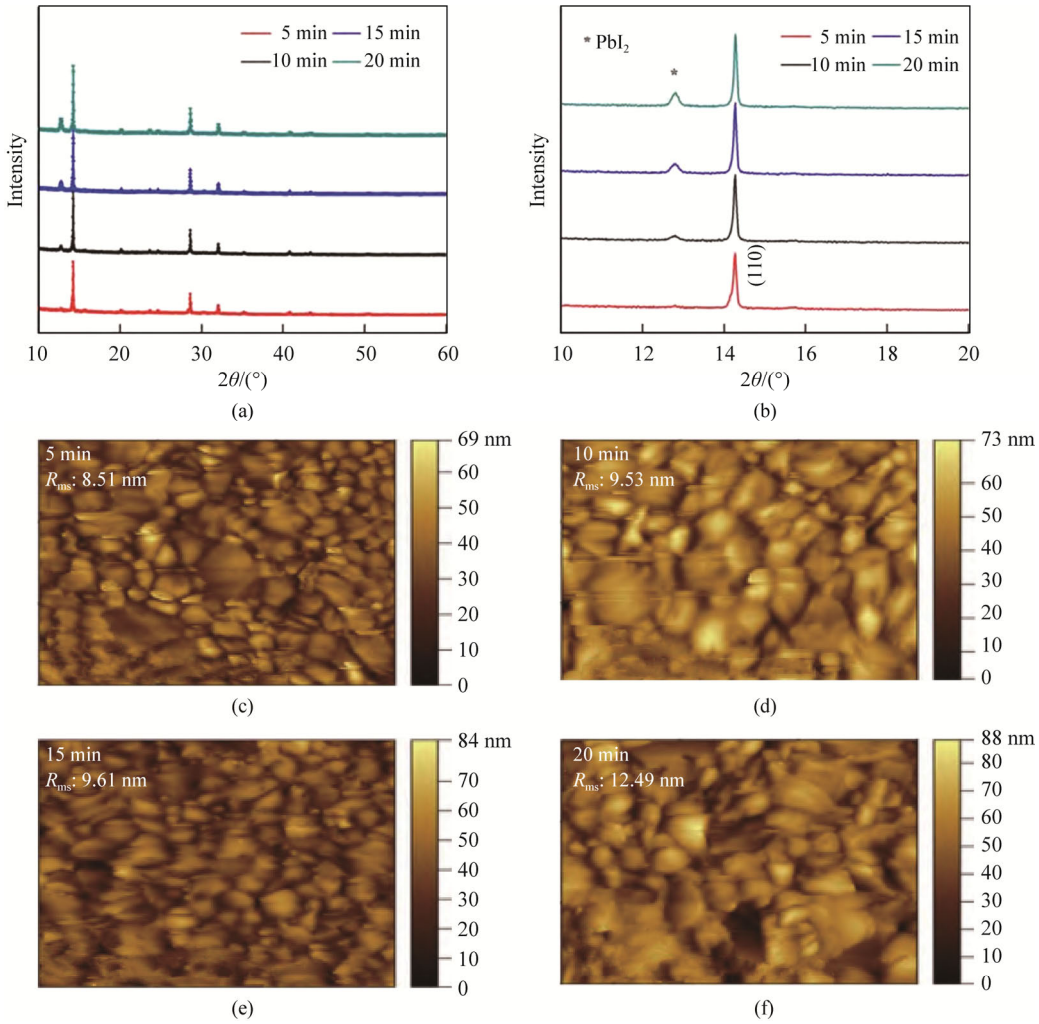


图 11 (a、b)钙钛矿的(XRD)谱[68]；(c～f) 4 种不同退火时间条件下制备的钙钛矿薄膜的 AFM 图[68]

Fig. 11 (a, b) XRD patterns of perovskite; (c–f) The atomic force microscopy (AFM) images of perovskite thin films prepared under four different annealing times[68]

通常，在相同退火温度下，钙钛矿晶粒随退火时间的延长而长大。Cao 等[25]研究发现，当退火时间从 5 s 延长到 10 s 时，晶粒尺寸明显增大。因此，优化退火时间是提高钙钛矿晶粒尺寸的常用途径。根据不同阶段的平均晶粒尺寸计算粗化速率。在 100 ℃退火的样品，平均尺寸在 5 s 内从 79.9 nm 增加到 91.3nm，如图 12a～图 12f 所示，对应的粗化速率为 2.28 nm/s。175 ℃和 250 ℃退火后，薄膜的粗化率分别提高到 32.26 nm/s 和 42.56 nm/s。当退火温度从 100 ℃升高到 250 ℃时，粗化速率提高了 18 倍以上。最终导致 PSCs 器件整体性能(开路电压、短路电流密度、填充因子及光电转换效率)均显著提升，如图 12g～图 12j 所示。

Ralaiarisoa 等[69]研究了退火时间对 $CH_3NH_3PbI_{3-x}Cl_x$ 混合卤化物钙钛矿薄膜的影响。退火的早期阶段，整个薄膜呈现出相分离的特征。随着退火时间的延长，溶液处理的钙钛矿薄膜从以横向分离的 $MAPbI_3$ 钙钛矿和富氯化铅为特征的不均匀成分演变为在 100 ℃下退火 100 min 后对应完全结晶的钙钛矿的单相。同时强调了 $PbCl_2$ 在引发钙钛矿成核中的关键作用以及 $MAPbCl_3$ 对形成高度均匀和纹理化的钙钛矿薄膜的重要性，这对获得高性能钙钛矿太阳能电池至关重要。另外，作者发现持续退火引发 MA 含量的相对不足会改变电子结构，并随着退火时间的增加促进 n 型薄膜的形成。该研究证实了氯在溶液处理混合卤化物 $MAPbI_{3-x}Cl_x$ 钙钛矿薄膜形成中的关键作用及其对钙钛矿基太阳能电池光电性能的影响，强调了控制退火条件和持续时间对优化钙钛矿薄膜制备的重要性。

Yao 等[70]通过研究发现，MAI-PbI_2-DMSO 中间相退火前的延迟时间在中间相中钙钛矿晶粒的成核过程中起着重要作用。随着退火前延迟时间

的延长，钙钛矿晶粒的成核数增加，晶粒尺寸变小，光照条件下从钙钛矿层注入电子传输层的载流子数量减少，因此器件性能会恶化。该项研究主要关注钙钛矿薄膜中 MAI-PbI_2-DMSO 中间相退火前的延迟时间，对 PSCs 器件的研究具有很强的参考价值。

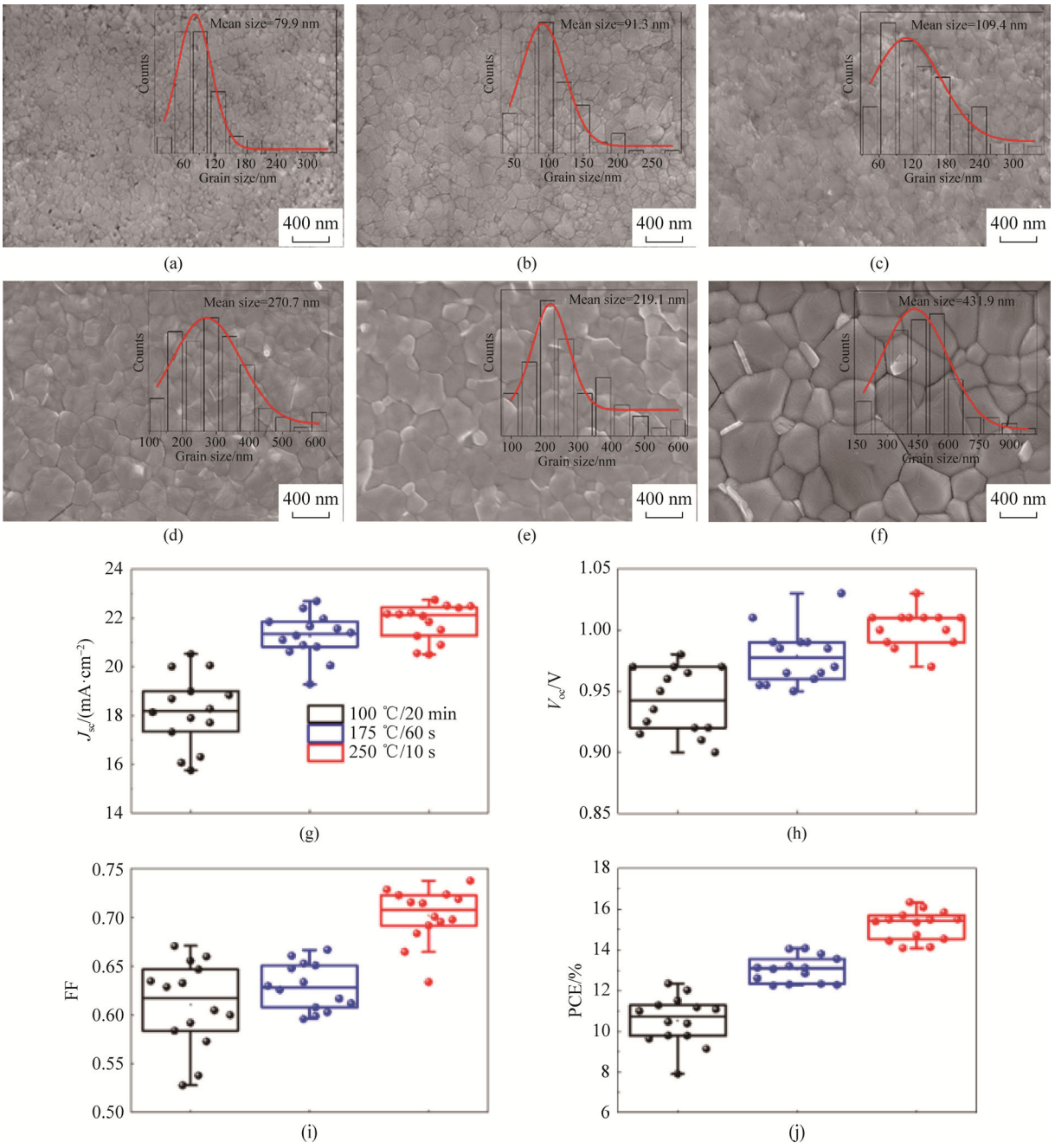


图 12　在不同温度下退火 5 s(左)和 10 s(右)的钙钛矿前驱体颗粒的演变[25]。(a)和(b)100 ℃，(c)和(d)175 ℃，(e)和(f)250 ℃，插图是相应钙钛矿薄膜的颗粒分布；器件 PSC 光伏参数的统计结果[25]，(g)短路电流密度 J_{sc}，(h)开路电压 V_{oc}，(i)填充因子 FF，(j)光电转换效率 PCE

Fig. 12　Evolution of the perovskite precursor grains annealed for 5 s (left) and 10 s (right) at different temperatures[25]. (a) and (b) 100 ℃, (c) and (d) 175 ℃, (e) and (f) 250 ℃. Insets are grain distribution of the corresponding perovskite films. Statistical results of photovoltaic parameters of the PSCs extracted from a series of devices[25]. (g) Short-circuit current density (J_{sc}), (h) open-circuit voltage (V_{oc}), (i) fill factor (FF), (j) photoelectric conversion efficiency (PCE)

Natik 等[71]通过实验和理论计算研究了退火时间对 $MAPbI_3$ 性能的影响。研究表明在 110 ℃的退火温度下分别经过 1 h 和 3 h 的退火后仍存在中间相，且随着退火时间的增加，中间相转化为钙钛矿。

在 4 h 退火后，中间相完全转变为钙钛矿，钙钛矿的形态也发生了改变，棒状晶粒的直径随着退火时间的增加而增加。研究表明，随着退火时间的增加，晶格收缩。因此可以推断退火时间对钙钛矿的纯度和物理性质的变化有显著的影响。Tian 等[72]在研究退火时间对三元阳离子(CsFAMA)钙钛矿薄膜及其太阳能电池的影响时发现，在室温添加 Cs 阳离子可以自发形成黑色 α 相，但后续的退火处理对钙钛矿薄膜的影响至关重要。在 100 ℃退火约 45 min 或 60 min 的三元阳离子(CsFAMA)钙钛矿薄膜较为理想。当退火时间进一步延长时，器件的 *J*–*V* 迟滞现象加剧。这主要是由于退火时间太长，使得离子迁移加剧以及钙钛矿分解致使 PbI_2 过量存在，导致电荷载流子输运不平衡。

Zhang 等[73]通过优化退火时间协调柔性钙钛矿太阳能电池的效率。图 13 a 和图 13b 展示了刚性 PSCs 和柔性 PSCs 在不同退火参数下的效率分布。对于刚性 PSC，在 150 ℃下持续 15 min 的时间可得 21.15%的最高效率。低于 120 ℃的温度容易导致钙钛矿内的有机前体溶剂不完全挥发，导致埋底界面中缺陷产生，从而显著限制器件的效率。由图 13 可见，对于刚性 PSCs，实现最佳性能的退火时间窗口相对宽松。通过在 120～170 ℃的温度范围内改变退火时间 12～24 min，成功获得了效率超过 21%的高效刚性 PSCs。相比之下，柔性 PSCs 的最佳性能只能在退火温度的狭窄范围内实现，特别是在 145～155 ℃之间。这一限制源于，更高的退火温度会导致柔性基板上钙钛矿晶粒的膨胀和变形。通过缩短退火时间(30～300 s)，在图 13c 中绘制了效率随时间的分布图。在长达 180 s 的持续时间内，观察到 PCE 和退火时间呈正相关的关系；超过 180 s 后，PCE 水平呈稳定趋势。这反映出退火时间对 PSCs 器件性能的总体影响，该项研究的发现为实现柔性 PSCs 的退火工艺和高效率的协调途径提供了一条实用且直接的指导依据。

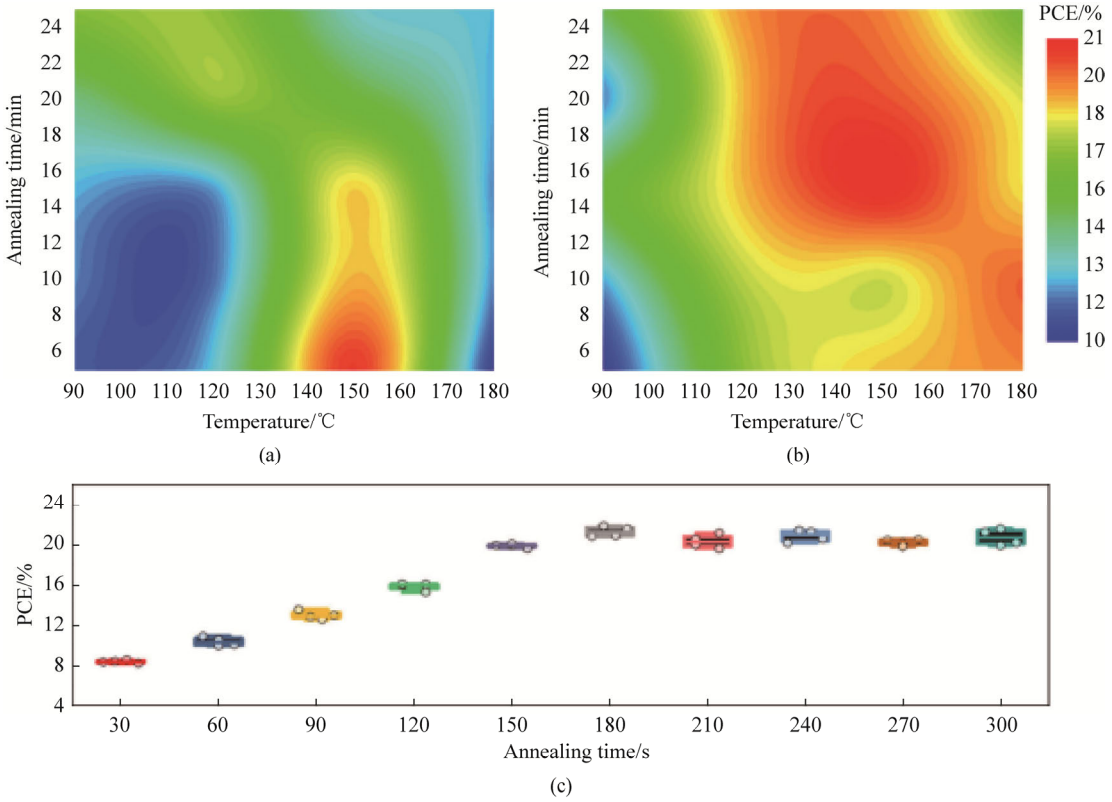


图 13 退火时间为 5～30 min、退火温度为 90～180 ℃的(a)柔性 PSCs 和(b)刚性 PSCs 的效率分布图；(c)在 150 ℃的退火温度下，退火时间在 30～300 s 内的效率分布图[73]

Fig. 13 Efficiency distribution maps corresponding to (a) flexible PSCs and (b) rigid perovskite solar cells with annealing time of 5–30 min and annealing temperature of 90–180 ℃, respectively; (c) efficiency distribution diagram of annealing time in 30–300 s at an annealing temperature of 150 ℃[73]

3.3 退火环境气氛

在钙钛矿薄膜的退火工艺中，除了退火温度、退火时间会对薄膜及器件性能产生关键影响外，退火环境气氛也是不可忽略的一个重要因素。通常情

况下，实验室制备钙钛矿薄膜及 PSCs 的过程是在手套箱中的惰性气氛(氮气)中操作的，这不利于商业化规模发展。主要原因在于钙钛矿太阳能电池的大面积低成本生产通常涉及在各种气氛中加工钙钛矿。因此，应当在更有利于促进 PSCs 产业化方向发展的条件下制备 PSCs。而改善钙钛矿薄膜的退火环境气氛就是极好的尝试。一般来讲，钙钛矿薄膜的退火环境气氛包括真空、惰性气体(氮气)、有机溶剂蒸汽、环境空气或一定湿度(水蒸气)等。研究表明，调控环境气氛在一定程度下对钙钛矿薄膜退火效果产生非常有利的影响[74–84]。

在真空环境下对钙钛矿薄膜进行退火，既可以避免退火过程的环境气氛对钙钛矿薄膜造成损伤，进而影响薄膜的光电性能，又有助于形成致密且结晶性能良好的钙钛矿薄膜[79–81]。Xie 等[74]提出真空辅助热退火是控制 $PbCl_2$ 和 CH_3NH_3I 前驱体形成 $CH_3NH_3PbI_3$ 薄膜成分和形态的有效手段，并确定了 CH_3NH_3Cl 副产物对钙钛矿薄膜的形成和光伏性能的关键作用。通过真空辅助热退火方法完全去除副产物，如图 14a 和图 14b 所示[74]，制备出纯度高且无孔的平面 $CH_3NH_3PbI_3$ 薄膜。所得器件效率高达 14.5%，同时去除 CH_3NH_3Cl 显著提高了器件的稳定性和重复性。Liu 等[75]比较了在真空和氮气环境中退火的 $CH_3NH_3Sn_{0.5}Pb_{0.5}I_xCl_{3-x}$ 薄膜后，发现真空辅助热退火使 $CH_3NH_3Sn_{0.5}Pb_{0.5}I_xCl_{3-x}$ 薄膜具有更好的薄膜覆盖率和结晶度。该过程加速甲基氯化铵的升华，降低 $CH_3NH_3Sn_{0.5}Pb_{0.5}I_xCl_{3-x}$ 薄膜中的陷阱密度。最后成功制备了低带隙钙钛矿太阳能电池，效率超过 12%，器件重复性和长期稳定性均很突出。Yu 等[28]证明了真空中进行热退火是调节由 PbI_2、CsI 和二甲基碘化铵(DMAI)前驱体形成的 $CsPbI_3$ 钙钛矿薄膜的形态和结晶度的有效方法。通过这种方法制备了大面积、高质量的 $CsPbI_3$ 薄膜。如图 15c～图 15f[28]所示，与 N_2 环境氛围退火的薄膜相比，真空退火的薄膜孔隙大幅降低且更为平整，使得 PSCs 的效率从 17.26%提高到 20.06%，同时稳定性大幅度提升。

有研究者采用有机溶剂蒸汽环境氛围辅助退火，如二甲基亚砜(DMSO)[76–79]等。有机溶剂蒸汽退火不仅有利于重塑钙钛矿薄膜的表面形态，降低钙钛矿薄膜的表面缺陷，同时有助于获得穿过更大晶粒的薄膜，提升薄膜质量。DMSO 蒸汽已被证明在促进钙钛矿晶体生长方面具有出色的能力，这可能源于其对 $CH_3NH_3PbI_3$ 钙钛矿的高极性和高溶解

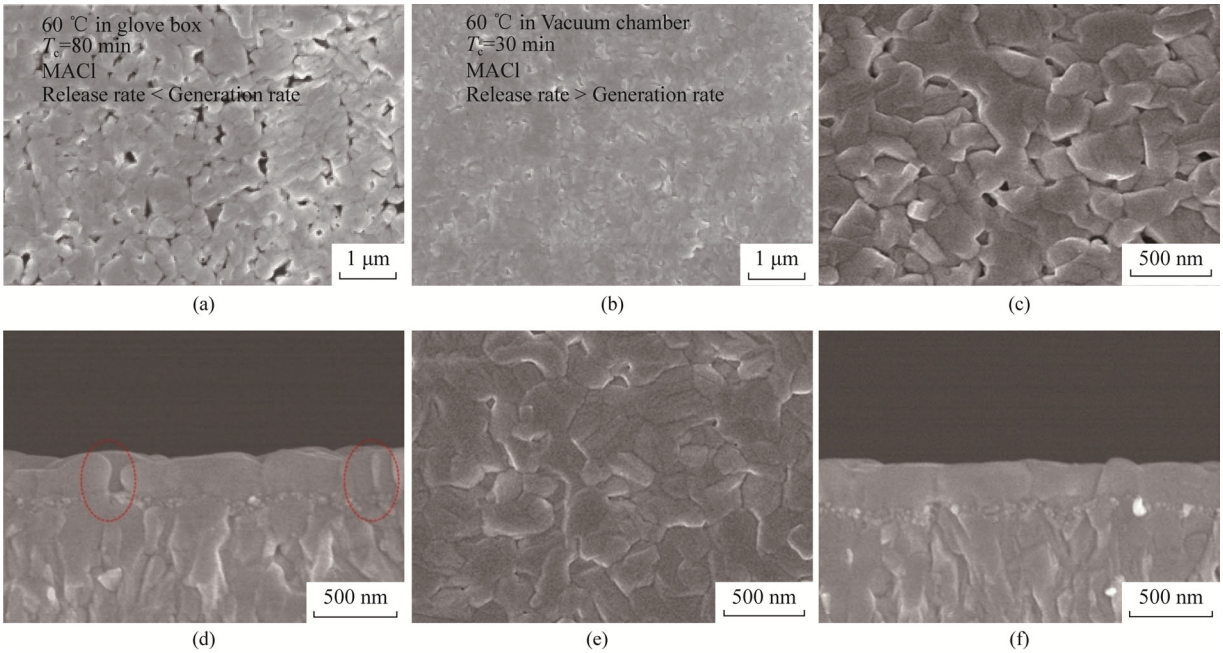


图 14　钙钛矿薄膜的 SEM 照片，在(a)手套箱和(b) 60 ℃真空室中热退火后，在 PEDOT:PSS/ITO 玻璃基板上形成的钙钛矿薄膜的 SEM 照片[74]；在(c)N_2 和(d)真空中退火的 $CsPbI_3$ 薄膜的顶面 SEM 照片；在(e)N_2 和(f)真空中退火的 $CsPbI_3$ 薄膜的横截面 SEM 照片[28]

Fig. 14　SEM images of the top surfaces of perovskite films[74]. SEM images of perovskite films formed on PEDOT:PSS/ITO glass substrates, after thermal annealing in (a) a glovebox and (b) a vacuum chamber at 60 ℃. Top-surface SEM images of the $CsPbI_3$ films annealed in (c) N_2 and (d) vacuum. Cross-sectional SEM images of the $CsPbI_3$ films annealed in (e) N_2 and (f) vacuum[28]

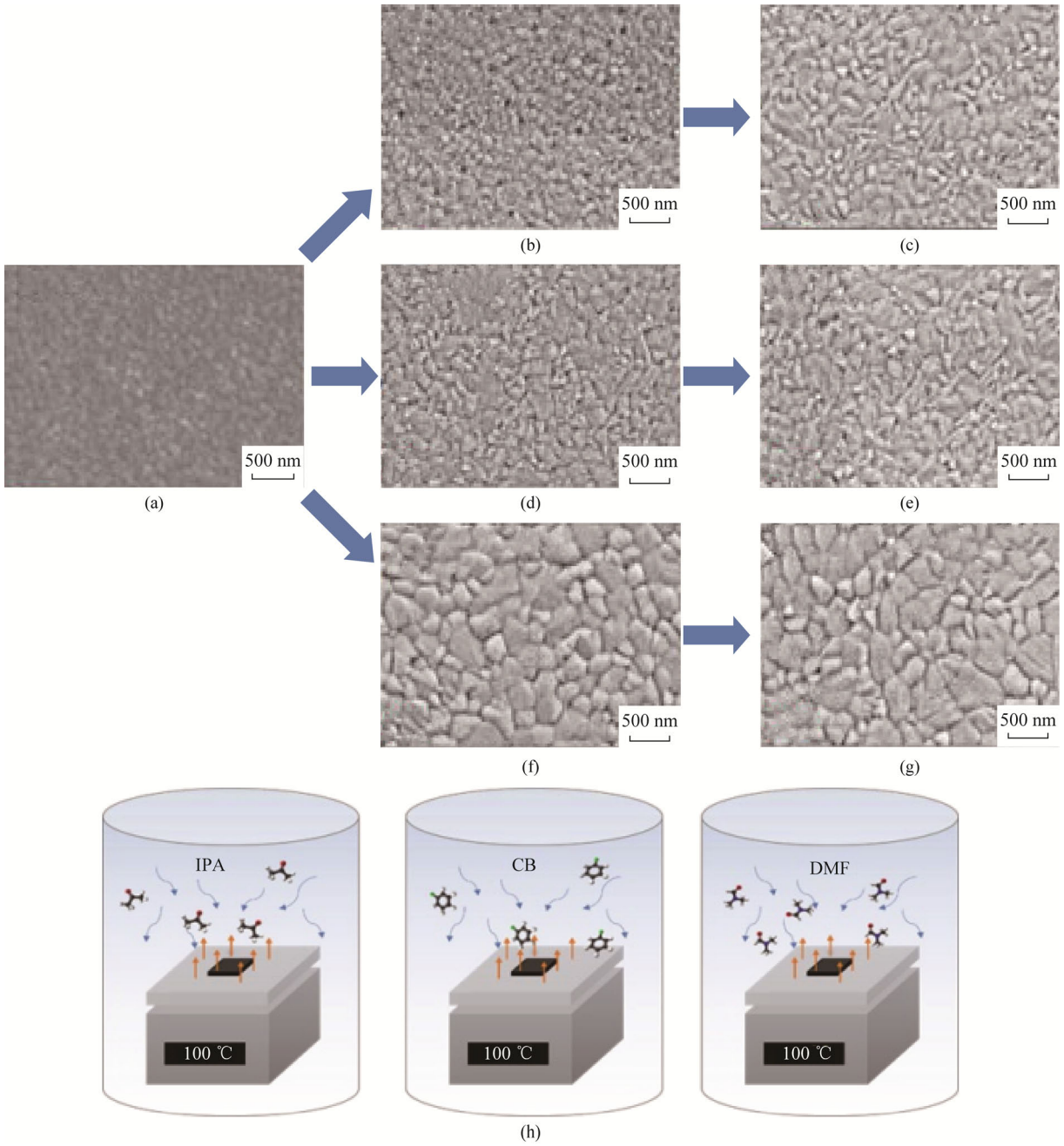


图 15 通过 SEM 测量在以下退火气氛中制备的不同钙钛矿薄膜的表面形貌：(a)未退火，(b) 10 min N_2，(c) 10 min 氮气和 20 min 空气，(d) 10 min 空气，(e) 30 min 和(f) 10 min DMSO，(g) 10 min DMSO+20 min 空气，图中比例尺是 500 nm[79]；(h)钙钛矿薄膜退火过程中气氛控制装置的示意图[86]

Fig. 15 Surface topography measured by SEM for different perovskite films fabricated in the atmosphere of (a) non-annealing, (b) 10 min N_2, (c) 10 min N_2 and 20 min air, (d) 10 min air, (e) 30 min, (f) 10 min DMSO, and (g) 10 min DMSO and 20 min air. Here, the scale bar is 500 nm[79]. (h) Schematic illustration of the atmosphere-controlled apparatus during perovskite film annealing[86]

度。纯氮气气氛往往导致 DMSO 溶剂的快速蒸发，从而导致依赖衬底的结晶过程，而 DMSO 气氛会减缓蒸发速率，导致与衬底无关的结晶过程[76]。Zhang 等[79]的研究表明，钙钛矿薄膜在不同气氛下在 100 ℃退火 10 min 后显示出截然不同的演变，如图 15 所示[79]。DMSO 蒸汽和空气组合的颗粒致密均匀，当在相同的空气气氛下进一步退火 20 min 时，每层薄膜的钙钛矿晶粒仅略有增加，如图 15c、图 15e 和图 15g 所示，其中 DMSO 处理薄膜仍然具有最大的晶粒，从而再次证实了初始薄膜状态对整个晶体生长过程的强烈影响。同时，该研究还强调了溶剂蒸汽也可能部分溶解制备的钙钛矿晶体的

情况，因此预计仅热退火过程的一定时间可以重建钙钛矿晶体。此外，N,N-二甲基甲酰胺(DMF)[80–83]、异丙醇(IPA)[84]、γ-丁内酯(GBL)[85]等溶剂也被用于溶剂蒸汽环境氛围辅助退火，并取得了良好的效果。

He 等[86]研究了 3 种常用溶剂蒸汽(包括 IPA、CB 和 DMF)退火对钙钛矿薄膜性能和器件性能的影响，如图 16h 所示。该研究发现，CB 可以通过去除其残留的 PbI_2 来改变自钝化钙钛矿结构，从而降低器件的开路电压。此外，IPA 蒸汽下退火会诱导薄膜产生 δ-钙钛矿，这将对薄膜及器件的性能产生不利影响。DMF 处理的薄膜则表现出最差的结晶度和薄膜质量，这可能会增加漏电流损失。这项工作强调了在钙钛矿退火过程中控制溶剂蒸汽气氛的重要性，为 PSCs 的实验室制备及产业化进程提供了不同的观点。

Chin 等[87]在研究通过溶剂蒸汽退火控制晶粒尺寸和结晶度来实现高发光钙钛矿薄膜时，分别将乙醇(EtOH)、水(H_2O)、N,N-二甲基甲酰胺(DMF)和二甲基亚砜(DMSO)用作溶剂蒸汽对钙钛矿薄膜进行退火。研究指出，极性溶剂处理通过 2 个同时进行的过程实现：再结晶过程，以及将未反应和剩余的前体转化为钙钛矿。研究发现，水(H_2O)是卤化物钙钛矿溶剂蒸汽退火工艺最合适的溶剂，可显著提高光致发光强度。Zia 等[88]通过调节退火气氛(氮气、空气和 MACl 蒸汽)来增强 $MAPbCl_3$ 结晶，发现过量的 MACl 蒸汽可以帮助获得形态均匀、表面完全覆盖的高质量 $MAPbCl_3$ 薄膜。

为了降低 PSCs 的制备成本，进而实现商业批量生产。有研究者将氮气氛围中钙钛矿退火的工艺过程延伸至工业生产环境，即空气环境。Pathak 等[89]发现，与在空气中退火的薄膜相比，在氮气氛围中退火的钙钛矿薄膜具有更高的电子无序度，进而光致发光寿命变短，器件性能变差。Wang 等[90]通过空气退火调节钙钛矿的结晶过程，导致高质量的二维钙钛矿薄膜具有较低的陷阱密度、良好的相分布和释放的残余应变。通过空气退火制备的所得器件实现了 18%的光电转换效率，同时证明了空气退火薄膜的热稳定性增强。Iqbal 等[7]在环境空气中退火的 $CsPbI_3$ 薄膜缺陷较少，环境空气退火在 $CsPbI_3$/HTM 界面诱导了能带弯曲增强，空气退火样品的电荷载流子提取得到改善，非辐射界面缺陷降低。因此，基于环境空气退火 $CsPbI_3$ 的 PSCs 的效率达 19.8%。这项研究为环境空气退火策略制备无机 PSCs 开辟了前景。在此基础上，为了提高 PSCs 在高湿度环境中的稳定性，有研究者在高湿度环境中制备高质量的钙钛矿薄膜，取得了良好的效果。Wang 等[91]通过在室温对 $CH_3NH_3PbI_3$ 进行水蒸气退火而不进行热退火，得到了高结晶度和无空隙的钙钛矿薄膜，所得器件光电转换效率达 16.4%。作者提出水蒸气分子催化了钙钛矿在晶粒边缘和空隙区域的溶解和再结晶，使得钙钛矿薄膜中无空隙和大尺寸的晶体，得到器件优异的光伏性能。该方法为平面 PSCs 的制造提供了一种简单、高效和节能的加工方法。Zou 等[92]通过研究发现，在湿度控制的环境中退火钙钛矿薄膜能有效抑制与 SnO_2 的去质子化反应，从而减少界面缺陷，提高载流子的提取效率和寿命。通过控制湿度，可以让水分在钙钛矿的生长过程中有选择性地吸附在(100)面上，促进了这一面晶体的生长。这种生长方式提高了晶体的质量，减少了 PbI_2 的生成。而在氮气氛围下，退火的钙钛矿会在钙钛矿和 SnO_2 界面发生强烈的去质子化反应，这会导致钙钛矿的分解和性能下降。而在湿度控制的氛围下，这种去质子化反应得到了有效抑制，显著降低了界面缺陷和 PbI_2 的生成。基于湿度退火的钙钛矿薄膜制备的 PSC 器件获得了 25.69%的光电转换效率，填充因子(FF)为 86.21%，并且在 1000 h 的持续太阳光照下，器件的稳定性没有明显衰减。该研究提出的湿度控制退火策略显著提升了钙钛矿太阳能电池的 PCE 和 FF，为下一代高效、稳定的钙钛矿太阳能电池提供了新途径。

3.4　退火温度、时间、气氛的协同作用

通常情况下，退火温度、时间、气氛三者并非各自独立地影响着钙钛矿薄膜的退火效果，而是三者协同调控，共同决定薄膜的结晶质量。通常，高温可加速结晶，但需严格控制时间(＜30 min)以避免晶界粗化和相分解；低温需通过延长退火时间(＞30 min)来保证结晶充分，否则易产生结晶不彻底或者残留非晶相的情况。惰性气体氛围中，如氮气，高温短时退火可以保护组分稳定性；活性氛围中，如在 O_2 氛围下，需低温(<100 ℃)持续适度时间的退火以钝化缺陷，其间需避免氧化副反应带来的消极影响。因此在钙钛矿薄膜的退火工艺中，退火温度、时间、氛围三者相互协同，共同影响钙钛矿薄膜的结晶动力学、缺陷态密度及器件性能。

3.5　影响钙钛矿薄膜退火效果的非工艺因素

除了 3.4 节所讨论的退火温度、时间、气氛 3 个工艺参数因素外，薄膜制备过程中的非工艺因素同

样不可忽略，主要表现为基底在退火过程中对薄膜的影响。基底的选择和预处理直接影响薄膜的结晶质量、形貌及器件性能。通常，基底材料的性质、基底形貌及基底与钙钛矿薄膜的界面相互作用等均会对钙钛矿薄膜退火效果产生影响。对于基底材料，主要考虑热膨胀系数、耐高温性、化学稳定性等。首先考虑基底与钙钛矿材料的热膨胀系数的匹配情况。倘若两者之间不匹配，则会导致薄膜退火过程中产生热应力，引发薄膜龟裂甚至剥离，因此科研人员往往采用铟锡氧化物(ITO)/玻璃等刚性基底。其次考虑基底的耐高温性。在高温退火时，柔性基底(主要是聚合物基底)容易变形或软化甚至分解，因此更多采用溶剂退火或者低温(＜100 ℃)退火。最后，基底材料是否与钙钛矿前驱溶液发生化学反应也是选择基底的关键因素。针对基底形貌，主要考虑其粗糙程度和孔隙情况。基底粗糙程度较高可能导致缺陷较多，适度粗糙度有利于在退火过程中增强成核密度，促进致密结晶；基底太光滑则不利于获得均匀覆盖的薄膜。例如在制备钙钛矿–晶硅叠层太阳能电池时，晶硅太阳能电池底电池采用绒面结构(微米级金字塔)以增强光捕获，但可能造成钙钛矿前驱体溶液填充不均，退火时溶剂挥发速率差异大，导致薄膜厚度不均或孔洞较多。此外，晶硅电池的钝化层(如 SiN_x、a-Si:H)耐受温度较低，高温退火会导致钝化层失效，因此在叠层电池钙钛矿薄膜退火时，还需兼顾晶硅基底电池、界面结构和退火工艺三者的相容性。如果是基底孔隙较多(介孔结构)，与高粗糙程度基底相似，可能会产生前驱溶液渗透不均匀，退火后薄膜缺陷较多。最后，基底表面官能团，如羟基、羧基等可与钙钛矿前驱体形成中间相，从而影响结晶动力学。

4 钙钛矿薄膜的无退火技术

目前，钙钛矿薄膜的退火工艺仍然具有一定的局限性，传统热退火技术产生针孔和裂纹，而新型退火技术的应用范围较窄，在批量/工业规模生产中广泛应用均存在很大困难，因此，通过退火工艺得到均匀结晶的大面积钙钛矿薄膜仍是一项挑战。因此，有部分科研工作者提出了无退火技术来解决这一难题，为高质量钙钛矿薄膜的结晶工艺提供了重要的借鉴，同时有利于降低钙钛矿太阳能电池的制备成本。

无退火技术通过完全避免退火步骤，依赖溶液法、原位结晶技术(如溶剂工程、添加剂调控、界面工程)等可直接形成高质量钙钛矿薄膜。如表 3 所示，与现有传统退火工艺和新型退火工艺相比，无退火工艺显著特征在于能够通过化学调控(如钙钛矿前驱液的添加剂)实现原位结晶，避免高温导致的晶界粗化，但晶粒尺寸往往低于高温退火样品。在工艺成本上，传统热退火工艺需高温炉，能耗大，耗时较长(5 min～1 h)且需惰性气体保护，工艺成本高且较为复杂；新型退火工艺的设备与能耗成本同样较高，对工艺要求较高，需要精确控制退火中的能量分布，但工艺时间较短，如激光退火数秒即可完成退火工艺；而无退火工艺无需退火设备，工艺成本低廉，节省能耗且兼容柔性基底，能够避免高温导致的基底变形。因此无退火工艺以低成本、高兼容性为核心优势，虽在晶粒尺寸上略逊于退火工艺，但通过工艺优化缩小差距，如界面工程，在柔性电子领域展现出不可替代的潜力。

表 3 无退火工艺与现有传统退火工艺和新型退火工艺的对比

Table 3 Comparison of non-annealing process with existing traditional annealing process and new annealing process

Process type	Characteristics
Traditional thermal annealing	The grain size is relatively large, typically ranging from several hundred nanometers to 1 micrometer. Moreover, the grain size distribution is wide and uneven, and continuous high-temperature conditions can easily lead to grain boundary coarsening.
New annealing	The grain size ranges from several tens to several hundred nanometers. By applying local or instantaneous energy input, the heat budget can be reduced (for example, the laser annealing time can be shortened to the millisecond level).
Non-annealing	The grain size is small and uniform, typically ranging from 10 to 100 nm. The grain size distribution is narrow, and the grain boundary compounding rate is high. The crystallization process is regulated by film formation kinetics (such as solvent evaporation rate and additive-induced crystallization).

据文献报道，前驱体溶液中的添加剂可以促成钙钛矿湿膜的结晶，可以避免额外的退火工艺，例如氯化铵(NH_4Cl)[93]、碘化胍(GAI)[94]。此外，也有人通过溶剂工程诱导结晶。Yin 等[95]将甲基碘化铵和碘化铅的溶液旋涂到基材上，并在旋涂过程中将乙酸乙酯滴到薄膜上，诱导 $CH_3NH_3PbI_3$ 钙钛矿薄膜瞬时结晶，所得钙钛矿薄膜显示出大尺寸晶粒和高载流子寿命的特征，同时该方法制备的无退火薄膜制备的 PSC 表现出与采用退火薄膜制得的 PSC 相当的性能。Fang 等[96]系统地研究了不同溶剂对钙

钛矿薄膜形态和结晶度的影响，开发了一种无需退火的均匀钙钛矿薄膜的溶剂技术。研究表明，N-甲基-2-吡咯烷酮(NMP)已被用作高沸点溶剂和络合剂，与 N, N-二甲基甲酰胺(DMF)或二甲基乙酰胺(DMAc)结合，形成中间相 MAI-PbI_2-NMP，室温反溶剂滴在薄膜上时，NMP 溶剂被迅速去除，促使钙钛矿薄膜立即成核和晶粒生长。该研究可能提供一种在室温制备高质量钙钛矿薄膜的新方法，这将简化制造过程并降低高效 PSC 制造的成本。Wang 等[97]用 2-甲氧基乙醇(2-ME)溶剂制备钙钛矿前驱体溶液，在手套箱中或室温在环境空气中旋涂后可以立即获得完全转化的钙钛矿薄膜，在手套箱中制备的 PSCs 器件的光电转换效率达 12.95%，在空气环境中的光电转换效率为 12.77%。这种非常简单、省时和低成本的方法为 PSCs 的商业化提供了一种新的思路。Dong 等[98]将 3,4-乙烯二氧噻吩(EDOT)引入反溶剂中，得到了无退火工艺制备的钙钛矿薄膜。EDOT 辅助的反溶剂策略有助于形成具有增大晶粒和减少缺陷的高质量钙钛矿薄膜，所得柔性和刚性 PSCs 器件分别取得了 15.58%和 20.12%的光电转换效率。

也有研究者通过界面工程实现钙钛矿薄膜的无退火工艺。Lou 等[99]在 SnO_2 和钙钛矿之间引入金属 Zr–有机框架(MOF)界面辅助工艺。研究发现，无需退火工艺，仅 Zr–MOF 界面就能够加速钙钛矿中间体的形成，促进其转化为钙钛矿晶体。该薄膜既不需要退火也不需要惰性气体保护，Zr-MOF 中的硫醇和羧基与 PbI_2 配位，加速了含 PbI_2 中间相转化为钙钛矿。研究发现，该方法制备的钙钛矿薄膜陷阱密度降低了约 1 倍，同时电子和空穴迁移率显著增加，从而增强了载流子提取并抑制了电荷复合。因此，基于 Zr–MOF 的 PSC 的光电转换效率达 20.24%，是参考器件(9.26%)的 2.2 倍。此外，Zr–MOF 界面层可以显着提高器件稳定性。在空气中储存 1018 h 后，基于 Zr–MOF 的器件光电转换效率保持在为初始效率的 93%，而参考器件的光电转换效率下降至初始效率的 52%。因此，Zr–MOF 界面无退火 $MAPbI_3$ 钙钛矿薄膜结晶度的提高是效率显著增强的根本原因。该项工作另辟蹊径地提出了一种无退火工艺制备钙钛矿薄膜的可行方法。

5　总结与展望

目前，退火工艺是钙钛矿薄膜结晶的常用手段，既有利于提高钙钛矿成膜过程中的成核率，也有利于增加薄膜的晶粒密度，且有利于形成较大且均匀分布的晶粒，得到高质量的钙钛矿薄膜，进而有利于提升器件的光伏性能。本研究系统综述了钙钛矿薄膜退火工艺的影响机制、退火方法种类、影响退火效果的工艺参数以及钙钛矿薄膜无退火技术的最新进展，旨在为高质量钙钛矿薄膜及高性能 PSCs 的制备提供理论依据和技术参考。

退火工艺通过优化钙钛矿薄膜的均匀性和覆盖率，促进晶粒生长并钝化界面缺陷，进而提升薄膜的结晶质量与光电性能。传统热退火工艺一定程度上提升钙钛矿薄膜质量，但这种溶液造成薄膜针孔以及晶粒尺寸不均匀等问题，一定程度上限制了 PSCs 的发展。因此一系列的新型退火技术被开发出来，如电磁波(红外光、紫外光、激光和微波)退火、超声退火、压力退火、溶剂退火等。此外，退火工艺参数的精准控制(如退火温度与升温速率、退火时间及退火环境气氛等)被证明是调节薄膜退火效果的关键，将直接影响器件的光伏性能。尽管退火工艺取得显著进展，其带来的副作用不可忽视。如高温退火易引发钙钛矿分解，部分退火工艺复杂且重复性较差，加之退火工艺带来的成本。因此，钙钛矿的无退火技术逐渐兴起，其不仅可以简化 PSCs 器件的工艺流程，且节省了退火过程的能耗，降低成本。然而，无退火薄膜的结晶质量仍与退火工艺仍有差距，未来仍需深入探索。

未来，钙钛矿薄膜退火工艺的研究很有可能有以下发展趋势。

第一，原位表征技术进一步发展，用于深入揭示退火过程中晶体生长的微观机制。

第二，借助机器学习的优势，高通量筛选高质量钙钛矿薄膜退火工艺数据，为高效钙钛矿太阳能电池的实验室制备及产业化应用提供技术指导。

第三，进一步开发钙钛矿薄膜的新型退火技术以及无退火技术，兼顾高效和低能耗的同步优化，在保障钙钛矿薄膜质量的同时，能够简化器件加工工艺和节省制作成本。

目前，钙钛矿太阳能电池产业化发展趋势日趋明显，尤以钙钛矿–晶硅叠层太阳能电池为主，迫切要求解决与工业级硅片兼容的大面积钙钛矿薄膜的均匀结晶难题，促使钙钛矿光伏的产业化进程迈向新阶段。

参考文献:

[1] KOJIMA A, TESHIMA K, SHIRAI Y, et al. Organometal halide perovskites as visible-light sensitizers for photovoltaic cells[J]. J Am

Chem Soc, 2009, 131(17): 6050–6051.

[2] National Renewable Energy Laboratory. Best research-cell efficiency chart (National Renewable Energy Laboratory, 2025)[EB/OL]. [2025–06–16]. https://www.nrel.gov/pv/interactive-cell-efficiency.html.

[3] WANG L, HUANG M Q, YU X F, et al. MOF-derived $Ni_{1-x}Co_x$@Carbon with tunable nano-microstructure as lightweight and highly efficient electromagnetic wave absorber[J]. Nanomicro Lett, 2020, 12(1): 150.

[4] YOUNG C, WANG J, KIM J, et al. Controlled chemical vapor deposition for synthesis of nanowire arrays of metal–organic frameworks and their thermal conversion to carbon/metal oxide hybrid materials[J]. Chem Mater, 2018, 30(10): 3379–3386.

[5] 沈文忠. 硅基异质结太阳电池物理与器件[M]. 李正平译. 北京: 科学出版社, 2014.

[6] WANG X, WANG H, SHAN T, et al. Fluorocarbon-based solvent-bath annealing for high-performance perovskite photovoltaics[J]. Adv Funct Mater, 2025, 35(3): 2413400.

[7] IQBAL Z, FÉLIX R, MUSIIENKO A, et al. Unveiling the potential of ambient air annealing for highly efficient inorganic $CsPbI_3$ perovskite solar cells[J]. J Am Chem Soc, 2024, 146(7): 4642–4651.

[8] MAITANI M M, ISO D, KIM J, et al. Microwave application to efficient annealing process of $CH_3NH_3PbI_3$ perovskite crystalline films[J]. Electrochemistry, 2017, 85(5): 236–240.

[9] LING P S V, HAGFELDT A, SANCHEZ S. Flash infrared annealing for perovskite solar cell processing[J]. J Vis Exp, 2021(168): e61730.

[10] WANG L, LIU G L, XI X, et al. Infrared photon-assisted annealing for crystal engineering in perovskite solar cells[J]. Bull Mater Sci, 2022, 45(2): 54.

[11] SANCHEZ S, HUA X, PHUNG N, et al. Flash infrared annealing for antisolvent-free highly efficient perovskite solar cells[J]. Adv Energy Mater, 2018, 8(12): 1702915.

[12] MARTIN B, YANG M J, BRAMANTE R C, et al. Fabrication of flexible perovskite solar cells *via* rapid thermal annealing[J]. Mater Lett, 2020, 276: 128215.

[13] KIM M, KIM G H, OH K S, et al. High-temperature–short-time annealing process for high-performance large-area perovskite solar cells[J]. ACS Nano, 2017, 11(6): 6057–6064.

[14] CRONIN H M, JAYAWARDENA K D G I, STOEVA Z, et al. Effects of ambient humidity on the optimum annealing time of mixed-halide Perovskite solar cells[J]. Nanotechnology, 2017, 28(11): 114004.

[15] LAMER V K, DINEGAR R H. Theory, production and mechanism of formation of monodispersed hydrosols[J]. J Am Chem Soc, 1950, 72(11): 4847–4854.

[16] SUN Y G. Controlled synthesis of colloidal silver nanoparticles in organic solutions: Empirical rules for nucleation engineering[J]. Chem Soc Rev, 2013, 42(7): 2497–2511.

[17] DUNLAP-SHOHL W, ZHOU Y Y, PADTURE N P, et al. Synthetic approaches for halide perovskite thin films[J]. Chem Rev, 2019, 119(5): 3193–3295.

[18] WHITEHEAD C, ÖZKAR S, FINKE R G. LaMer's 1950 model for particle formation of instantaneous nucleation and diffusion-controlled growth: A historical look at the model's origins, assumptions, equations, and underlying sulfur Sol Formation kinetics data[J]. Chem Mater, 2019, 31(18): 7116–7132.

[19] WANG L, LIU G L, XI X, et al. Annealing engineering in the growth of perovskite grains[J]. Crystals, 2022, 12(7): 894.

[20] QIN M C, TSE K, LAU T K, et al. Manipulating the mixed-perovskite crystallization pathway unveiled by *in situ* GIWAXS[J]. Adv Mater, 2019, 31(25): 1901284.

[21] WANG Z Y, CHEN P, LUO J W, et al. Gradient thermal annealing assisted perovskite film crystallization regulation for efficient and stable photovoltaic-photodetection bifunctional device[J]. Small Meth, 2025, 9(3): 2401098.

[22] ZHANG J, LIANG W S, YU W, et al. A two-stage annealing strategy for crystallization control of $CH_3NH_3PbI_3$ films toward highly reproducible perovskite solar cells[J]. Small, 2018, 14(26): 1800181.

[23] CHEN W J, CHEN H Y, XU G Y, et al. Precise control of crystal growth for highly efficient $CsPbI_2Br$ perovskite solar cells[J]. Joule, 2019, 3(1): 191–204.

[24] SONG Q, LIANG C J, ZHANG H M, et al. Additional organic-solvent-rinsing process to enhance perovskite photovoltaic performance[J]. Adv Electron Mater, 2019, 5(10): 1900244.

[25] CAO X B, ZHI L L, JIA Y, et al. High annealing temperature induced rapid grain coarsening for efficient perovskite solar cells[J]. J Colloid Interface Sci, 2018, 524: 483–489.

[26] SHARGAIEVA O, LANG F, RAPPICH J, et al. Influence of the grain size on the properties of $CH_3NH_3PbI_3$ thin films[J]. ACS Appl Mater Interfaces, 2017, 9(44): 38428–38435.

[27] YU G H, JIANG K J, GU W M, et al. Vacuum-assisted thermal annealing of $CsPbI_3$ for highly stable and efficient inorganic perovskite solar cells[J]. Angew Chem Int Ed, 2022, 61(27): e202203778.

[28] SHIN G S, CHOI W G, NA S, et al. Lead acetate based hybrid perovskite through hot casting for planar heterojunction solar cells[J]. Electron Mater Lett, 2018, 14(2): 155–160.

[29] LIAO H C, GUO P J, HSU C P, et al. Enhanced efficiency of hot-cast large-area planar perovskite solar cells/modules having controlled chloride incorporation[J]. Adv Energy Mater, 2017, 7(8): 1601660.

[30] SHARMA B, SINGH S, PAREEK S, et al. Radiative and conductive thermal annealing of hybrid organic-inorganic perovskite layer[J]. Sol Energy Mater Sol Cells, 2019, 195: 353–357.

[31] GÜNZLER A, BERMÚDEZ-UREÑA E, MUSCARELLA L A, et al. Shaping perovskites: *in situ* crystallization mechanism of rapid thermally annealed, prepatterned perovskite films[J]. ACS Appl Mater Interfaces, 2021, 13(5): 6854–6863.

[32] HUANG S H, GUAN C K, LEE P H, et al. Toward all slot-die fabricated high efficiency large area perovskite solar cell using rapid near infrared heating in ambient air[J]. Adv Energy Mater, 2020, 10(37): 2001567.

[33] SÁNCHEZ S, VALLÉS-PELARDA M, ALBEROLA-BORRÀS J A, et al. Flash infrared annealing as a cost-effective and low environmental impact processing method for planar perovskite solar cells[J]. Mater Today, 2019, 31: 39–46.

[34] OUYANG Z L, ABRAMS H, BERGSTONE R, et al. Rapid layer-specific annealing enabled by ultraviolet LED with estimation of crystallization energy for high-performance perovskite solar cells[J]. Adv Energy Mater, 2020, 10(4): 1902898.

[35] YOU P, LI G J, TANG G Q, et al. Ultrafast laser-annealing of perovskite films for efficient perovskite solar cells[J]. Energy Environ Sci, 2020, 13(4): 1187–1196.

[36] JEON T, JIN H M, LEE S H, et al. Laser crystallization of organic–inorganic hybrid perovskite solar cells[J]. ACS Nano, 2016, 10(8): 7907–7914.

[37] SONG C P, TONG L, LIU F, et al. Addressing the reliability and electron transport kinetics in halide perovskite film *via* pulsed laser engineering[J]. Adv Funct Mater, 2020, 30(5): 1906781.

[38] YANG H R, SONG C P, XIA T C, et al. Ultrafast transformation of PbI_2 in two-step fabrication of halide perovskite films for long-term performance and stability *via* nanosecond laser shock annealing[J]. J Mater Chem C, 2021, 9(37): 12819–12827.

[39] XU J, HU Z Y, JIA X Y, et al. A rapid annealing technique for efficient perovskite solar cells fabricated in air condition under high humidity[J]. Org Electron, 2016, 34: 84–90.

[40] BRITES M J, BARREIROS M A, CORREGIDOR V, et al. Ultrafast low-temperature crystallization of solar cell graded formamidinium-cesium mixed-cation lead mixed-halide perovskites using a reproducible microwave-based process[J]. ACS Appl Energy Mater, 2019, 2(3): 1844–1853.

[41] CHEN Q, MA T T, WANG F F, et al. Rapid microwave-annealing process of hybrid perovskites to eliminate miscellaneous phase for high performance photovoltaics[J]. Adv Sci, 2020, 7(12): 2000480.

[42] AHMADIAN-YAZDI M R, ESLAMIAN M. Toward scale-up of perovskite solar cells: Annealing-free perovskite layer by low-cost ultrasonic substrate vibration of wet films[J]. Mater Today Commun, 2018, 14: 151–159.

[43] ZHANG X, ZABIHI F, XIONG H, et al. Highly efficient flexible perovskite solar cells made *via* ultrasonic vibration assisted room temperature cold sintering[J]. Chem Eng J, 2020, 394: 124887.

[44] LI N X, NIU X X, LI L, et al. Liquid medium annealing for fabricating durable perovskite solar cells with improved reproducibility[J]. Science, 2021, 373(6554): 561–567.

[45] EPERON G E, HABISREUTINGER S N, LEIJTENS T, et al. The importance of moisture in hybrid lead halide perovskite thin film fabrication[J]. ACS Nano, 2015, 9(9): 9380–9393.

[46] RAGA S R, JUNG M C, LEE M V, et al. Influence of air annealing on high efficiency planar structure perovskite solar cells[J]. Chem Mater, 2015, 27(5): 1597–1603.

[47] YIN X T, GUO Y X, LIU J, et al. Moisture annealing effect on $CH_3NH_3PbI_3$ films deposited by solvent engineering method[J]. Thin Solid Films, 2017, 636: 664–670.

[48] XIAO Z G, DONG Q F, BI C, et al. Solvent annealing of perovskite-induced crystal growth for photovoltaic-device efficiency enhancement[J]. Adv Mater, 2014, 26(37): 6503–6509.

[49] LIU J, GAO C, HE X L, et al. Improved crystallization of perovskite films by optimized solvent annealing for high efficiency solar cell[J]. ACS Appl Mater Interfaces, 2015, 7(43): 24008–24015.

[50] FAN H C, HUANG J H, CHEN L S, et al. Methylamine-assisted secondary grain growth for $CH_3NH_3PbI_3$ perovskite films with large grains and a highly preferred orientation[J]. J Mater Chem A, 2021, 9(12): 7625–7630.

[51] TIAN L W, WEN F, ZHANG W F, et al. Rising from the ashes: Gaseous therapy for robust and large-area perovskite solar cells[J]. ACS Appl Mater Interfaces, 2020, 12(44): 49648–49658.

[52] LIU C, WANG K, YI C, et al. Efficient perovskite hybrid photovoltaics *via* alcohol-vapor annealing treatment[J]. Adv Funct Mater, 2016, 26(1): 101–110.

[53] MOU J P, SONG J, CHE M, et al. Butanol-assisted solvent annealing of $CH_3NH_3PbI_3$ film for high-efficient perovskite solar cells[J]. J Mater Sci Mater Electron, 2019, 30(1): 746–752.

[54] ZHENG H F, LIU Y Q, SUN J. Micron-sized columnar grains of $CH_3NH_3PbI_3$ grown by solvent-vapor assisted low-temperature (75 ℃) solid-state reaction: The role of non-coordinating solvent-vapor[J]. Appl Surf Sci, 2018, 437: 82–91.

[55] MOORE D T, SAI H, WEE TAN K, et al. Impact of the organic halide salt on final perovskite composition for photovoltaic applications[J]. APL Mater, 2014, 2(8): 081802.

[56] GUO X, MCCLEESE C, KOLODZIEJ C, et al. Identification and characterization of the intermediate phase in hybrid organic–inorganic $MAPbI_3$ perovskite[J]. Dalton Trans, 2016, 45(9): 3806–3813.

[57] DUALEH A, TÉTREAULT N, MOEHL T, et al. Effect of annealing temperature on film morphology of organic–inorganic hybrid pervoskite solid-state solar cells[J]. Adv Funct Mater, 2014, 24(21): 3250–3258.

[58] LIU Y H, AKIN S, HINDERHOFER A, et al. Stabilization of highly efficient and stable phase-pure $FAPbI_3$ perovskite solar cells by molecularly tailored 2D-overlayers[J]. Angew Chem Int Ed, 2020, 59(36): 15688–15694.

[59] ZHANG Y, SEO S, LIM S Y, et al. Achieving reproducible and high-efficiency (>21%) perovskite solar cells with a presynthesized $FAPbI_3$ powder[J]. ACS Energy Lett, 2020, 5(2): 360–366.

[60] HAQUE F, YI H M, DUAN L P, et al. Optimisation of annealing temperature for low temperature processed inverted structure caesium formamidinium lead triiodide perovskite solar cells[J]. Mater Sci Semicond Process, 2019, 102: 104580.

[61] FROLOVA L A, ANOKHIN D V, PIRYAZEV A A, et al. Highly efficient all-inorganic planar heterojunction perovskite solar cells produced by thermal coevaporation of CsI and PbI_2[J]. J Phys Chem

Lett, 2017, 8(1): 67–72.

[62] AHMAD W, KHAN J, NIU G D, et al. Inorganic $CsPbI_3$ perovskite-based solar cells: A choice for a tandem device[J]. Sol RRL, 2017, 1(7): 1700048.

[63] LIU C, YANG Y, XIA X, et al. Soft template-controlled growth of high-quality $CsPbI_3$ films for efficient and stable solar cells[J]. Adv Energy Mater, 2020, 10(9): 1903751.

[64] TAGUCHI M, SUZUKI A, OKU T, et al. Effects of annealing temperature on decaphenylcyclopentasilane-inserted $CH_3NH_3PbI_3$ perovskite solar cells[J]. Chem Phys Lett, 2019, 737: 136822.

[65] CHANG Y T, TIEN C H, LEE K Y, et al. Evaporated $MAPbI_3$ perovskite planar solar cells with different annealing temperature[J]. Energies, 2021, 14(8): 2145.

[66] 符祥, 周凯, 钱艳楠. 退火温度对碳基全无机钙钛矿太阳能电池性能的影响[J]. 材料研究与应用, 2023, 17(2): 338–341.
FU Xiang, ZHOU Kai, QIAN Yannan. Mater Res Appl, 2023, 17(2): 338–341.

[67] WARGULSKI D R, XU K, HEMPEL H, et al. Relationship between the annealing temperature and the presence of PbI_2 platelets at the surfaces of slot-die-coated triple-halide perovskite thin films[J]. ACS Appl Mater Interfaces, 2023, 15(35): 41516–41524.

[68] 王娇宇, 熊健, 张哲泠, 等. 退火时间对平面型倒置钙钛矿太阳能电池性能的影响[J]. 桂林电子科技大学学报, 2022, 42(2): 154–160.
WANG Jiaoyu, XIONG Jian, ZHANG Zheling, et al. J Guilin Univ Electron Technol, 2022, 42(2): 154–160.

[69] RALAIARISOA M, BUSBY Y, FRISCH J, et al. Correlation of annealing time with crystal structure, composition, and electronic properties of $CH_3NH_3PbI_{3-x}Cl_x$ mixed-halide perovskite films[J]. Phys Chem Chem Phys, 2017, 19(1): 828–836.

[70] YAO Y J, ZOU X P, CHENG J, et al. Impact of delay time before annealing MAI-PbI_2-DMSO intermediate phase on perovskite film quality and photo-physical properties[J]. Crystals, 2019, 9(3): 151.

[71] NATIK A, MOUBAH R, ABID Y, et al. Annealing time effects on the structural, morphological and optical properties in hybrid $CH_3NH_3PbI_3$ perovskites: Experimental and *ab*-initio investigations[J]. Opt Mater, 2020, 109: 110255.

[72] TIAN L W, ZHANG W F, HUANG Y L, et al. Effects of annealing time on triple cation perovskite films and their solar cells[J]. ACS Appl Mater Interfaces, 2020, 12(26): 29344–29356.

[73] ZHANG Y, SHI Y F, WANG H N, et al. Harmonizing efficiency and bending performance in flexible perovskite solar cells through annealing duration optimization[J]. Energy Technol, 2024, 12(6): 2301316.

[74] XIE F X, ZHANG D, SU H M, et al. Vacuum-assisted thermal annealing of $CH_3NH_3PbI_3$ for highly stable and efficient perovskite solar cells[J]. ACS Nano, 2015, 9(1): 639–646.

[75] LIU M Y, CHEN Z M, XUE Q F, et al. High performance low-bandgap perovskite solar cells based on a high-quality mixed Sn–Pb perovskite film prepared by vacuum-assisted thermal annealing[J]. J Mater Chem A, 2018, 6(34): 16347–16354.

[76] XIU Y L, LIU Y, NIU K, et al. Solvent-vapor atmosphere controls the *in situ* crystallization of perovskites[J]. ACS Materials Lett, 2021, 3(8): 1172–1180.

[77] ZOU D Y, WANG Y P, ZHANG Y, et al. Solvent atmosphere-assisted crystallization of perovskites for room-temperature continuous-wave amplified spontaneous emission[J]. J Mater Chem C, 2023, 11(34): 11730–11738.

[78] XIAO S, BAI Y, MENG X Y, et al. Unveiling a key intermediate in solvent vapor postannealing to enlarge crystalline domains of organometal halide perovskite films[J]. Adv Funct Mater, 2017, 27(12): 1604944.

[79] ZHANG L X, TIAN S, YU Z H, et al. Rational solvent annealing for perovskite film formation in air condition (July 2017)[J]. IEEE J Photovolt, 2017, 7(5): 1338–1341.

[80] YANG X D, LIU D B, LI P, et al. The N, N-dimethylformamide annealing for enhanced performance of perovskite solar cells fabricated in ambient air[J]. Nano, 2018, 13(9): 1850102.

[81] GUO Z L, ZHUANG J, MA Z, et al. Improving the performance of lead acetate-based perovskite solar cells *via* solvent vapor annealing[J]. CrystEngComm, 2019, 21(32): 4753–4762.

[82] GAME O S, SMITH J A, ALANAZI T I, et al. Solvent vapour annealing of methylammonium lead halide perovskite: What's the catch?[J]. J Mater Chem A, 2020, 8(21): 10943–10956.

[83] ZHONG Y, SEEBERGER D, HERZIG E M, et al. The impact of solvent vapor on the film morphology and crystallization kinetics of lead halide perovskites during annealing[J]. ACS Appl Mater Interfaces, 2021, 13(38): 45365–45374.

[84] ZHAO X M, LIU T R, KAPLAN A B, et al. Accessing highly oriented two-dimensional perovskite films *via* solvent-vapor annealing for efficient and stable solar cells[J]. Nano Lett, 2020, 20(12): 8880–8889.

[85] LUO J, QIU R Z, YANG Z S, et al. Mechanism and effect of γ-butyrolactone solvent vapor post-annealing on the performance of a mesoporous perovskite solar cell[J]. RSC Adv, 2018, 8(2): 724–731.

[86] HE M, CHEN S Y, WANG T R, et al. Effects of solvent vapor atmosphere on photovoltaic performance of perovskite solar cells[J]. Crystals, 2023, 13(4): 549.

[87] CHIN S H, CHOI J W, WOO H C, et al. Realizing a highly luminescent perovskite thin film by controlling the grain size and crystallinity through solvent vapour annealing[J]. Nanoscale, 2019, 11(13): 5861–5867.

[88] ZIA W, MALEKSHAHI BYRANVAND M, RUDOLPH T, et al. $MAPbCl_3$ light absorber for highest voltage perovskite solar cells[J]. ACS Energy Lett, 2024, 9(3): 1017–1024.

[89] PATHAK S, SEPE A, SADHANALA A, et al. Atmospheric influence upon crystallization and electronic disorder and its impact on the photophysical properties of organic–inorganic perovskite solar cells[J]. ACS Nano, 2015, 9(3): 2311–2320.

[90] WANG B X, BI S Q, CHENG Q, et al. Air annealing facilitates crystallization reconstruction of quasi-2D perovskite[J]. Sol RRL, 2023,

7(3): 2201032.

[91] WANG B B, ZHANG Z G, YE S Y, et al. Room-temperature water-vapor annealing for high-performance planar perovskite solar cells[J]. J Mater Chem A, 2016, 4(44): 17267–17273.

[92] ZOU S W, ZHANG J J, XIN Y, et al. Moisture-inhibited deprotonation at the buried interface enables efficient perovskite solar cells with a high fill factor of over 86%[J]. Energy Environ Sci, 2025, 18(7): 3385–3394.

[93] CHEN Y N, ZHAO Y X, LIANG Z Q. Non-thermal annealing fabrication of efficient planar perovskite solar cells with inclusion of NH_4Cl[J]. Chem Mater, 2015, 27(5): 1448–1451.

[94] DONG H, PANG S Z, HE F Q, et al. Annealing-free, high-performance perovskite solar cells by controlling crystallization *via* guanidinium cation doping[J]. Sol RRL, 2021, 5(7): 2100097.

[95] YIN M S, XIE F X, CHEN H, et al. Annealing-free perovskite films by instant crystallization for efficient solar cells[J]. J Mater Chem A, 2016, 4(22): 8548–8553.

[96] FANG X, WU Y H, LU Y T, et al. Annealing-free perovskite films based on solvent engineering for efficient solar cells[J]. J Mater Chem C, 2017, 5(4): 842–847.

[97] WANG G, LIAO L P, CHEN L J, et al. Perovskite solar cells fabricated under ambient air at room temperature without any post-treatment[J]. Org Electron, 2020, 86: 105918.

[98] DONG C, CHEN J, CHEN C H, et al. Annealing-free perovskite films by EDOT-assisted anti-solvent strategy for flexible indoor and outdoor photovoltaics[J]. Nano Energy, 2022, 94: 106866.

[99] LOU L Y, WAN L, WANG Z S. MOF-assisted annealing-free crystallization technology of perovskites toward efficient and stable perovskite solar cells[J]. ACS Appl Mater Interfaces, 2023, 15(30): 37059–37068.

Annealing Process of Perovskite Thin Films in Perovskite Solar Cells

MENG Wenbing[1], *Tayirjan·TURERSUN*[1], *HE Minghua*[1], *ZHANG Linrui*[2,3], *NING Jun*[2,3]

(1. School of Mathematics and Physics, Xinjiang Hetian College, Hetian 848000, Xinjiang, China; 2. College of Physics and Electronic Information, Inner Mongolia Normal University, Hohhot 010022, China; 3. Inner Mongolia Key Laboratory for Applied Condensed Matter Physics, Hohhot 010022, China)

Extended Abstract

Perovskite solar cells (PSCs) have grown into a research hotspot in the field of photovoltaics due to their exceptional optoelectronic properties. The photovoltaic performance of PSCs is directly influenced by the perovskite thin film as the light-absorption layer of the device. Generally, the growth conditions of perovskite crystals are one of the primary factors for the quality of the perovskite film. The photovoltaic performance of PSCs is critically dependent on the quality of the perovskite film, in which the annealing method plays a pivotal role in the fabrication process. During the formation of high-quality perovskite crystals, the role of annealing is primarily to remove solvents from the wet perovskite film and promote the crystallization of film. The different annealing methods and processes vary in their effectiveness of facilitating film growth.

This article reviews recent advancement in annealing for perovskite thin films in PSCs, with a particular emphasis on prevalent annealing methods and the critical process factors governing the final film quality and device performance. First, the annealing process and its mechanism in promoting the crystallization of perovskite films is introduced. Second, the principal annealing methods reported to date for perovskite crystallization are summarized, including traditional thermal annealing, improved thermal annealing techniques, and novel annealing technologies. Third, the critical process parameters included the synergistic effects of temperature, time, and annealing atmosphere and non-process factors involved the properties of the substrate material for governing the annealing results are systematically discussed. Subsequently, the development of annealing-free techniques for perovskite films is examined. Finally, the future research directions for the annealing process of perovskite thin films are outlined, with the aim of supporting the commercialization of perovskite solar cells.

Summary and Prospects

The annealing process for perovskite thin films helps to increase the nucleation rate during film formation, then enhances the grain density, and subsequently promotes the formation of larger and uniformly distributed grains, and ultimately results in high-quality perovskite films, thereby improving the photovoltaic performance of the devices. This article systematically reviews the influencing mechanisms of the annealing process, the types of annealing methods, the process parameters affecting annealing outcomes, and the latest advancements in annealing-free techniques for perovskite thin films. The aim is to provide theoretical foundations and technical references for the preparation of high-quality perovskite films and high-performance PSCs.

By optimizing the uniformity and coverage of perovskite films, the annealing process promotes grain growth and passivates interface defects, thereby enhancing the crystalline quality and optoelectronic properties of the films. While traditional thermal annealing improves film quality to some extent, it can also lead to issues such as pinholes and uneven grain size, which limit the development of PSCs. Consequently, a variety of novel annealing techniques have been developed, including electromagnetic wave (infrared, ultraviolet, laser, and microwave) annealing, ultrasonic annealing, pressure annealing, and solvent annealing. Moreover,

precise control of annealing parameters—such as temperature, heating rate, duration, and ambient atmosphere—has been proven critical to optimizing annealing outcomes and directly influences the photovoltaic performance of the devices.

Despite significant progress in annealing techniques, their side effects cannot be overlooked. For instance, high-temperature annealing may trigger perovskite decomposition, some methods are complex and lack reproducibility, and the process incurs additional costs. As a result, annealing-free techniques are gaining attention, as they simplify the fabrication process of PSCs, reduce energy consumption, and lower costs. However, the crystalline quality of annealing-free films still lags behind that of annealed films, warranting further exploration.

Looking ahead, research on the annealing process for perovskite thin films is likely to develop in the following directions:

First, further advancement of *in-situ* characterization techniques to deeply reveal the microscopic mechanisms of crystal growth during annealing.

Second, leveraging the advantages of machine learning for high-throughput screening of annealing process data to guide the laboratory preparation and industrial application of high-efficiency PSCs.

Third, continued development of novel annealing and annealing-free techniques that balance efficiency and low energy consumption, ensuring high film quality while simplifying the fabrication process and reducing costs.

Currently, the industrialization of perovskite solar cells is becoming increasingly prominent, particularly in perovskite-silicon tandem solar cells. There is an urgent need to address the challenge of achieving uniform crystallization of large-area perovskite films compatible with industrial-grade silicon wafers, which will propel the industrialization of perovskite photovoltaics to a new stage.

Keywords perovskite solar cells; perovskite films; annealing; crystaline quality